MAGiC - Preliminary System Design

Version 0.2

SUMMARY **4**

1 INTRODUCTION **5**

1.1 PURPOSE OF THE DOCUMENT 5

1.2 ABBREVIATION 5

2. SYSTEM CHARACTERISTICS **6**

2.1 SYSTEM PURPOSE 6

2.2 SYSTEM OVERVIEW 6

3. INSTRUMENT OVERVIEW **7**

3.1 INSTRUMENT LAYOUT 7

3.2 TABLE OF COMPONENT POSITIONS 8

3.3 MAGIC P&ID 9

4. BEAM TRANSPORT AND CONDITIONING SYSTEM (13.6.18.1) **10**

4.1 NEUTRON OPTICS 10

4.1.1 Details of the baseline of neutron optics *10*

4.1.2 Neutron Beam Extraction System (13.6.18.1.1) *11*

4.1.3 Solid state bender (13.6.18.1.5.1.1) *12*

4.1.4 Elliptic super-mirrors (13.6.18.2.1) *13*

4.1.5 Beam geometry conditioning (13.6.18.1.4) *16*

4.2 CHOPPERS (13.6.18.1.3) 17

4.2.1 Chopper Pit 1: Pulse Shaping Chopper and 14 Hz Overlap Chopper *19*

4.2.2 Band Chopper *20*

4.2.3 Mode of operation *22*

4.2.4 Failures *22*

4.2.5 Chopper Control System *22*

4.3 POLARIZATION (13.6.18.1.5 & 13.6.18.3.1) 23

4.3.1 Thermal neutron polarization *23*

4.3.2 Cold neutron polarization (13.6.18.1.5.4) *23*

4.3.3 Polarization analysis *24*

4.3.4 Spin handling *27*

5 SAMPLE EXPOSURE AND CHARACTERIZATION SYSTEM **30**

5.1 SAMPLE ENVIRONMENT (13.6.18.2.3) 30

5.1.1 Dimensions *30*

5.1.2 Devices *31*

5.2 RADIAL COLLIMATOR (13.6.18.3.4) 31

5.3 DETECTORS (13.6.18.2.3.2) 32

5.3.1 Efficiency *33*

5.3.2 Resolution *33*

5.3.3 Fallback option *34*

5.4 MONITORS (13.6.18.1.6) 34

6 EXPERIMENTAL CAVE (13.6.18.5) 36
6.1 GEOMETRY 36
6.2 INFRASTRUCTURE (13.6.18.5.3) 37
6.3 SHIELDING (13.6.18.5.4) 38
6.4 SAMPLE CAVE ACCESS STRATEGY 38
6.5 PERSONNEL SAFETY SYSTEM (13.6.18.5.1) 38
7 SHIELDING (13.6.18.1.9) 39
7.1 IN-BUNKER SHIELDING (13.6.18.1.9.1) 39
7.1.1 Shielding of thermal neutrons 39
7.1.2 Shielding of high energy neutrons and prompt γ pulse 39
7.2 HIGH ENERGY SHUTTER (13.6.18.1.7.2) 40
7.3 NEUTRON GUIDE SHIELDING (13.6.18.1.9.3) 41
7.3.1 High energy: first half-ellipse 42
7.3.2 High energy: thermal Polarizer 43
7.3.3 High energy: second half-ellipse 43
7.4 EXPERIMENTAL CAVE SHIELDING 44
7.3.1 Fast shutter 44
7.3.2 Beam stop 44
7.3.3 γ and scattered neutrons shielding 44
8 PRELIMINARY SAFETY ANALYSIS FOR THE INSTRUMENT 46
9 SOFTWARE COMPONENTS 47
9.1 INSTRUMENT CONTROL 47
9.2 DATA VISUALIZATION 47
9.3 DATA REDUCTION 47
9.4 DATA ANALYSIS 48
10 EXPECTED PERFORMANCE AT 2 MW 50
10.1 DIFFUSE MAGNETIC SCATTERING INCLUDING POLARIZATION ANALYSIS 50
10.2 STRUCTURE DETERMINATION USING POLARIZED NEUTRONS 51

SUMMARY

This document describes the preliminary engineering design of the MAGiC single crystal diffractometer at a level of detail sufficient for preliminary design. This document provides an overview of the instrument and refers to Technical Solution Description documents for further details. The expected performance of the chosen technical solutions with respect to the functional requirements is shown, followed by an evaluation of the scientific performance.

1 Introduction

1.1 Purpose of the document

The Preliminary System Design Description of the MAGiC instrument describes the system architecture and the physical layout of the instrument. The hardware and software descriptions result from the design work based on the functional requirements (1) as well as the constraint requirements that have been identified at this point. The purpose of this document, together with the System Requirements and Concept of Operations documents is to:

- Provide a documented description of the design of the instrument that can be reviewed and approved by the stakeholders in a Tollgate review,
- Provide a description of the instrument in enough detail that its component parts can be designed in detail ("design-to specification"),
- Provide a description of the hardware and software system components in sufficient detail to assess whether they fulfil the functional requirements
- Discuss the expected scientific performance of the instrument

1.2 Abbreviation

PBS	:	Product Breakdown Structure
NOSG	:	Neutron Optics and Shielding Group
BTS	:	Beam Transport and Conditioning System
SES	:	Sample Exposure System
SCS	:	Scattering Characterization System
CEA	:	Commissariat à l'énergie atomique
CNRS	:	Centre national de la recherche scientifique
LLB	:	Laboratoire Léon Brillouin
JCNS	:	Jülich Center for Neutron Science
PSI	:	Paul Scherrer Institute
GUI	:	Graphical user interface
CLI	:	Command line interface
EPICS	:	Experimental Physics and Industrial Control System
PSS	:	Personnel Safety System

2. System Characteristics

2.1 System purpose

The MAGiC instrument is a polarized single crystal diffractometer with polarization analysis optimized for low volume (< 1mm3) single crystals and/or epitaxial films. MAGiC will primarily serve the broad magnetism community and has been designed with upgradability and flexibility in mind. The complete scientific case supporting the instrument is described in the instrument proposal [1] and covers the topics of multi-functional materials, fundamental magnetism, superconductivity, epitaxial films with the possibility to explore new trends to come in magnetism.

2.2 System overview

The instrument consists of three main technical subsystems: the beam transport and conditioning system (BTS), the sample exposure system (SES) and the scattering characterization system (SCS). In addition, as described in the instrument product breakdown structure (PBS), the instrument includes the structures that house and support these subsystems, the software to control the instrument and the software to process the data. The hardware description in this document does not strictly follow the PBS, but rather a functional breakdown of technical components along the neutron beam path. This makes it easier to map the specifications to the high level scientific requirements. PBS numbers are given for reference where appropriate.

3. Instrument overview

3.1 Instrument layout

A full overview of the MAGiC instrument is shown in Figure 3.1. There are four main areas starting from the source; inside the bunker, between bunker and guide hall (D01), in the guide hall, and in the experimental hall (E03).

The main components within the bunker are the Beam Extraction System, the Pulse Shaping and Selection Choppers, the first part of the guide system and its associated guide field, the solid-state bender and the high-energy neutron shutter. The instrument vacuum system begins at the position of the γ shutter.

Outside of the bunker wall starts the instrument shielding enclosing the guide system up to the experimental cave. At mid-distance the elliptic guide is interrupted by a three-meter-long straight part ensuring thermal neutron polarization. The band chopper will be located next to the thermal polarizer, sharing the same shielding. An adiabatic spin-flipper will be located along the guide path, outside of the experimental cave.

The experimental cave houses the last portion of the guide system and the optional focusing device, the sample exposure system and the beam characterization system with detector and polarization analyzers.

The control hutch will house the necessary equipment and network connection to ensure smooth operation of the instrument. A sample preparation lab including all the necessary equipment to prepare, mount and store single crystals will also be located next to the control hutch.

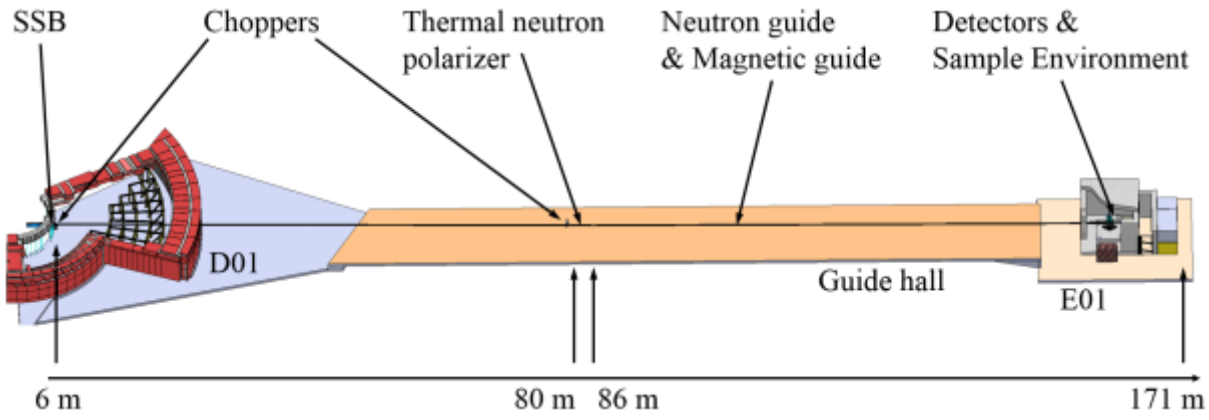

Fig. 3.1: *aerial view of the MAGiC instrument.*

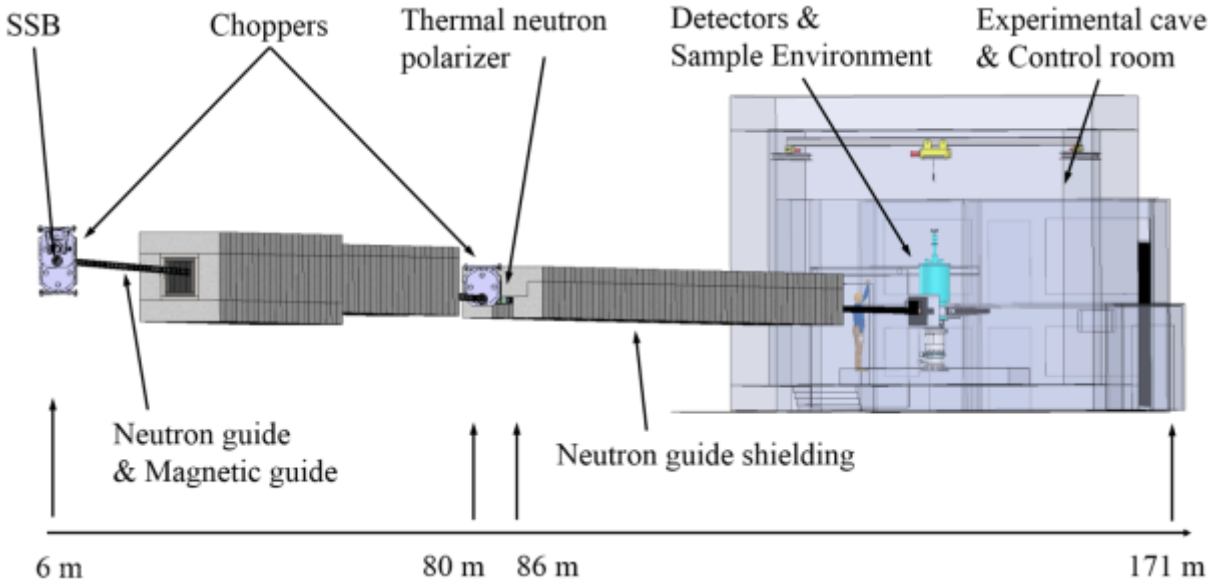

Fig 3.2: *perspective view of the MAGiC instrument showing the various components transporting and shaping the neutron beam up to the experimental cave.*

3.2 Table of component positions

The following table summarizes the geometrical parameters and positions of the most important components of MAGiC. The distance is defined from the instrument focal point focal point with the x-axis along the main beam axis, the y-axis in the horizontal plane and the z-axis vertical.

Item	Category	Defining parameters (e.g. WxHxL) [mm]	Start from origin [mm]	End from origin [mm]
Tapered NBES channel	Flight path	WxH = 124x30 to 40x30	2000	5500
γ Shutter	Shutter	L = 590	5510	6000
Solid State Bender	Polarizing bender	30x30x50	6200	6250
Pulse Shaping Chopper	Disk Chopper	D = 450; opening = 180°	6240	6240
Selection chopper	Chopper	D=480;	6700	6700
First guide section	Elliptic guide	L=74000; m<=4	6900	80900
Heavy Shutter	Shutter	L=1500	23000	24500
Band chopper	Chopper	D=700; opening=180°	80000	80000
Polarizer	Channeled guide	L=3000; nchan=6; m=4	80900	83900
Fourth guide section	Elliptic guide	L=74000; m<=4	83900	157500
RF spin flipper	Flipper	L=1000	149000	150000
Focusing device	Elliptic guide	L=1000; m<=6	157900	158900
Sample volume	SE	D=800	159000	159800
Sample position	Sample		159400	159400
Radial collimator 1	Collimator	H=500; L=240; open=160°	159800	160040
Detector 1	^{10}B detector	H=500; L=300; open=60°	160400	160900
Polarization analyzer	Super-mirrors	H=150; L=100; open=120°	160300	160400
Detector 2	^{10}B detector	H=150; L=300; open=120°	160400	160900
Beamstop (B_4C+Pb)	Absorber	WxHxL = 400x400x400	163500	163900

3.3 MAGiC P&ID

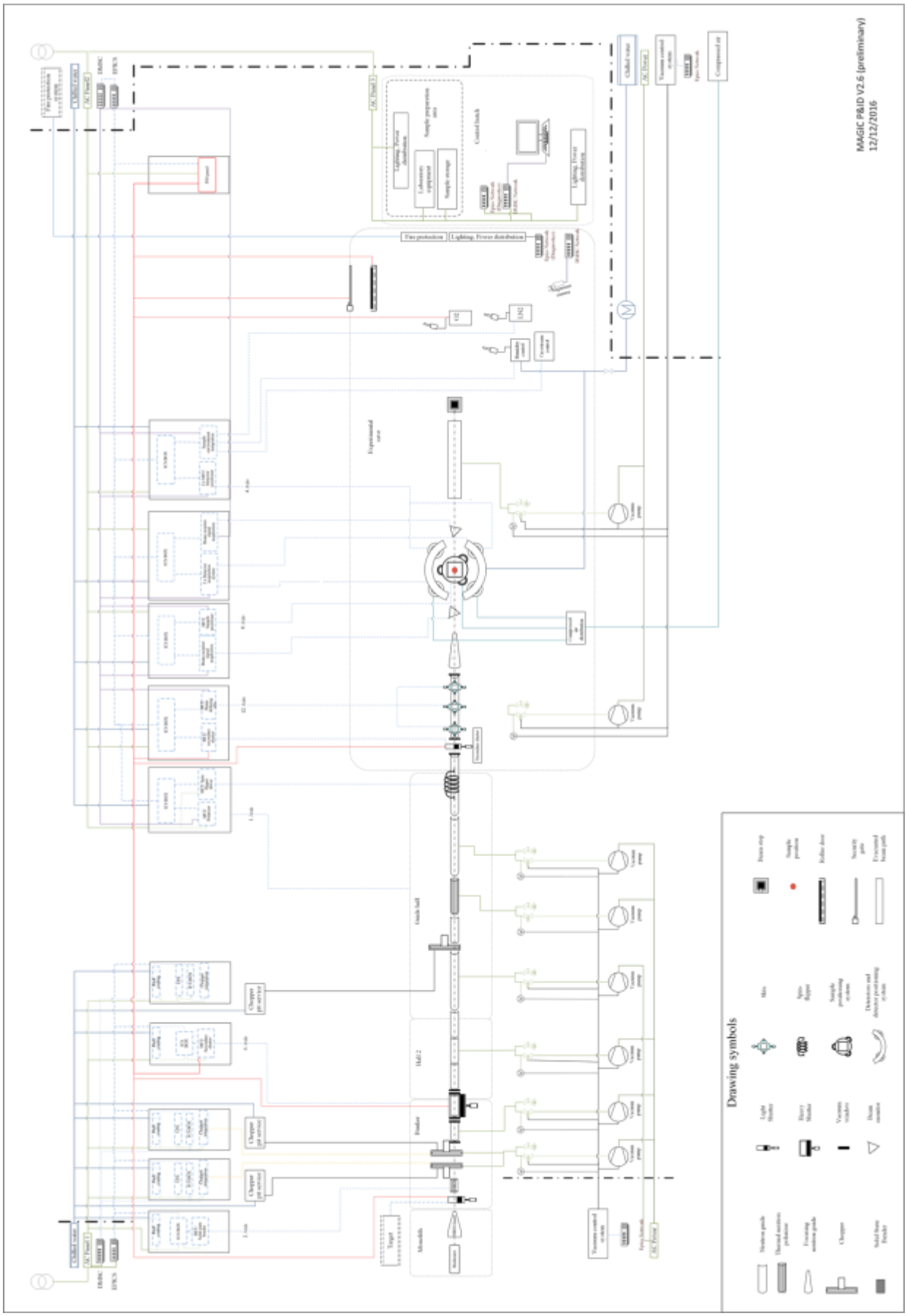

4. Beam Transport and Conditioning System (13.6.18.1)

The neutron optics system consists of the beam extraction system (PBS 13.6.18.1.1), beam delivery system (PBS 13.6.18.1.2), beam geometry conditioning (PBS 13.6.18.1.4) and beam filtering system (PBS 13.6.18.1.5). Their common purpose is to transport the neutron beam with reflective elements from the moderator to the sample exposure system (PBS 13.6.18.2).

4.1 Neutron Optics

The neutron optics is composed of the Neutron Beam Extraction System in the monolith, the cold solid state bender, the elliptic guide, the thermal polarizer and an incident beam collimation device. The complete neutron optics system has been optimized with the following Figure of Merit (FoM) in agreement with the System Requirements Documentation:

- Collimation: +/-0.30°
- Homogeneous area: 5x5 mm^2.
- Wavelength: $0.6 < \lambda < 6$ Å

The collimation can be either reduced or increased. To increase collimation, the foreseen technical solution will be identical to the DREAM's one and will consist in the insertion of slits in the last section of the guide, close to the guide exit. Varying of collimation is one of the key system requirements for MAGiC. A highly collimated beam is needed to study long magnetic periodicity compounds for which the transversal Q-resolution has to match the highest available time resolution. On the opposite, the ability to increase divergence at sample position is mandatory to increase flux on X-ray sized single crystals. In the last case of micrometric sample, an optional component will be installed between the guide exit and the sample position to increase the flux on smaller sample, focusing the beam on a 1x1 mm^2 sample with an incident divergence of +/-1°.

The guide itself has been optimized for highest possible transport and polarization of the thermal spectrum within the FoM described above. To maximize thermal neutrons transport, a 151 m long straight elliptic guide geometry is the most efficient one. However, to maximize polarization over the whole spectrum and avoid the direct line of sight from the moderator, the ellipse is vertically kinked by 0.23° in two places, at 80.5 and 83.5 m, forcing a polarizing reflection.

4.1.1 Details of the baseline of neutron optics

The moderator used during the optimization process was the BF2 one. Since then, a new BF1 geometry has been proposed changing the position of the focal point. The coordinate system used for optimization on MAGiC has its origin on the West focal point. Some minor changes may be necessary to accommodate this new design. (see Figure 4.1.1).

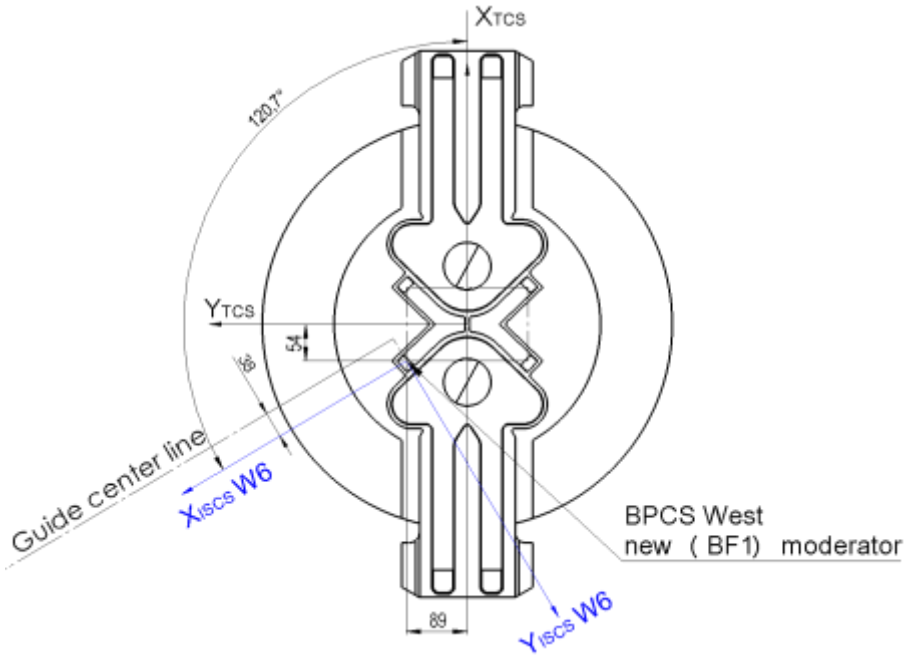

Figure 4.1.1: *The BF2 moderator model and change of BPCS for the new moderator BF1. The W6 coordinate system is represented in blue. The guide main axis is shifted by 38 mm, facing the thermal moderator (dashed line).*

4.1.2 Neutron Beam Extraction System (13.6.18.1.1)

The beam extraction system is oriented to the top-moderator, looking directly at the W6 focal point, and will allow extraction of both cold and thermal spectra. The moderator phase space to extract is limited to a 5x5 mm^2 area and a 0.6°x0.6° divergence range. As such, no optics is necessary in the NBES to ensure high brilliance transfer and the current design is limited to a 124x30 mm channel in a steel/copper insert. To reduce the cost of shielding, the guide system in its entirety is inclined with a -0.46° slope starting from the moderator (see also fig. 4.1.2). The NBES characteristics are summarized in the following table:

Distance (m)	Width (mm)	Height (mm)	Z rotation (°)	Y rotation (°)
2,00	124	30	0	-0.46
5,50	41	30	0	-0.46

The use of super-mirrors for the cold moderator could help as the current design is optimized for the BF1 focal point. During the first years, the focal point will be shifted horizontally by 21 mm. This change has no effect on the thermal performance of MAGiC. A small loss in brilliance is to be expected in the cold spectrum.

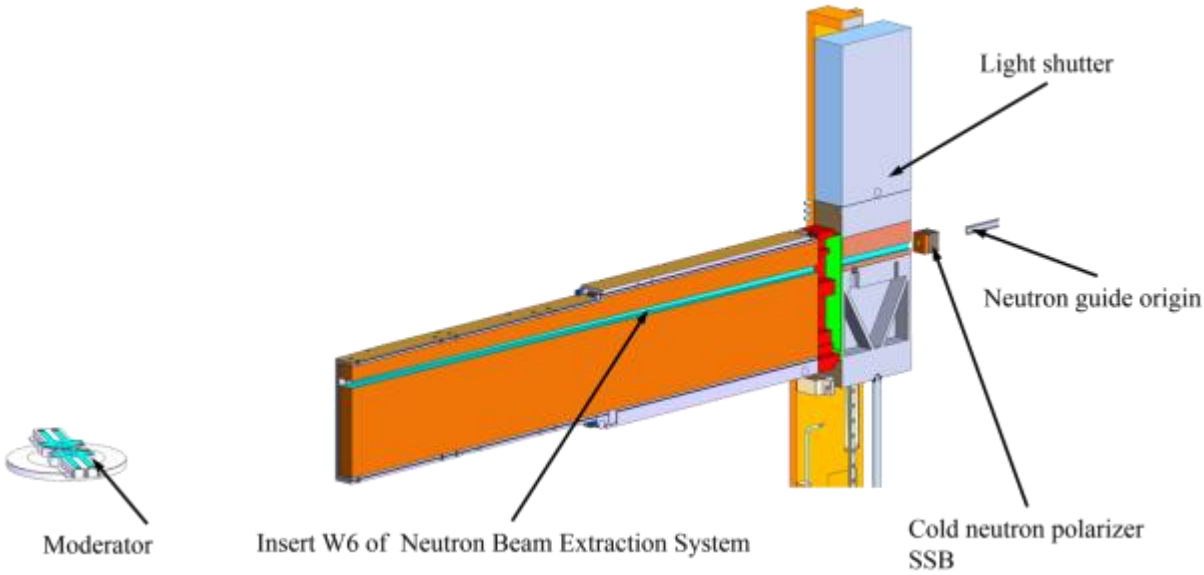

Figure 4.1.2: *3D model of the MAGiC NBES. The green part corresponds to the tapered channel with the negative slope clearly visible.*

4.1.3 Solid state bender (13.6.18.1.5.1.1)

The solid-state bender will be used to inject cold neutrons inside the elliptic guide system. The bender will be composed of 150 μm thick silicon wafer coater. On the reflective side, the wafers will be coated with *m*=4 FeSi while the non-reflective one will be coated with a Gd_2O_3 layer. Each wafer will therefore act as a channel for cold neutrons and will be bent with a curvature radius of 3.4 m. The external dimensions of the bender are 30x50x30mm (WxDxH) (see fig. 4.1.3.1).

The bender will be placed on a kinematic mount at 6200 mm from the focal point. An alternate solution would be to design a second light shutter channel with high positioning precision and to enclose the SSB in the light shutter. The SSB will then be placed at 5350 mm for focal point. If it is technically feasible, efficient and robust, this solution will be our favored choice.

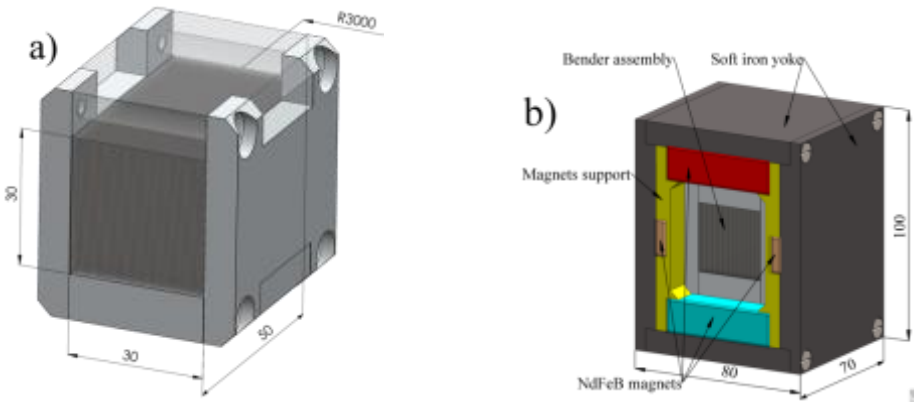

Fig. 4.1.3.1. *a) Solid state bender assembly with external dimensions; b) Magnetic assembly of the bender.*

Due to silicon absorption, the brilliance transfer of the SSB is reduced based on its thickness. On the cold neutron spectrum, the estimated absorption for a 5-cm thick bender is of 7 to 15% (see fig. 4.1.3.2). Note that in this calculation the extinction from a bended silicon crystal has not been taken into account.

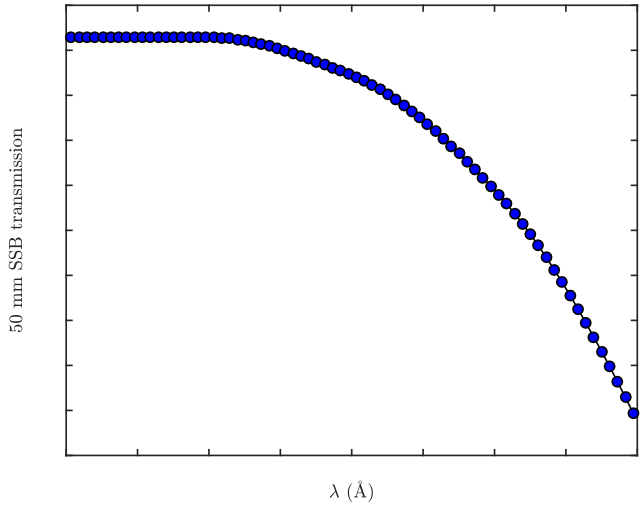

Figure 4.3.1.2: *transmission of a 5-cm thick silicon block versus wavelength.*

4.1.4 Elliptic super-mirrors (13.6.18.2.1)

The elliptic parameters of the guide have been optimized to maximize the transportation of 0.6A neutrons within the FoM while providing a high polarization rate.

Following requirements from the NOSG handbook, the guide substrate is 6-mm thick aluminum inside the bunker and 5 mm thick N-BK7 outside of the bunker. The guide will be enclosed in a vacuum housing such that vacuum constraints will be supported by the housing.

Each 2-m long guide section will be aligned inside the vacuum housing prior to installation. The final guide alignment on site will be manually made directly on the housing.

4.1.4.1 Geometry

The guide geometry has been optimized using ideal *m*=4 super-mirrors in McStas on the BF2 moderator design. A numerical collimation of +/-0.3° was used in front of a 5x5 mm^2 λ detector to account for the FoM. The calculated intensities for each wavelength bins were compared to the source ones defining the Brilliance Transfer of the iteration. The best iteration was kept as the optimal solution. A schematic view of the retained geometry is presented in figure 4.1.4.1.

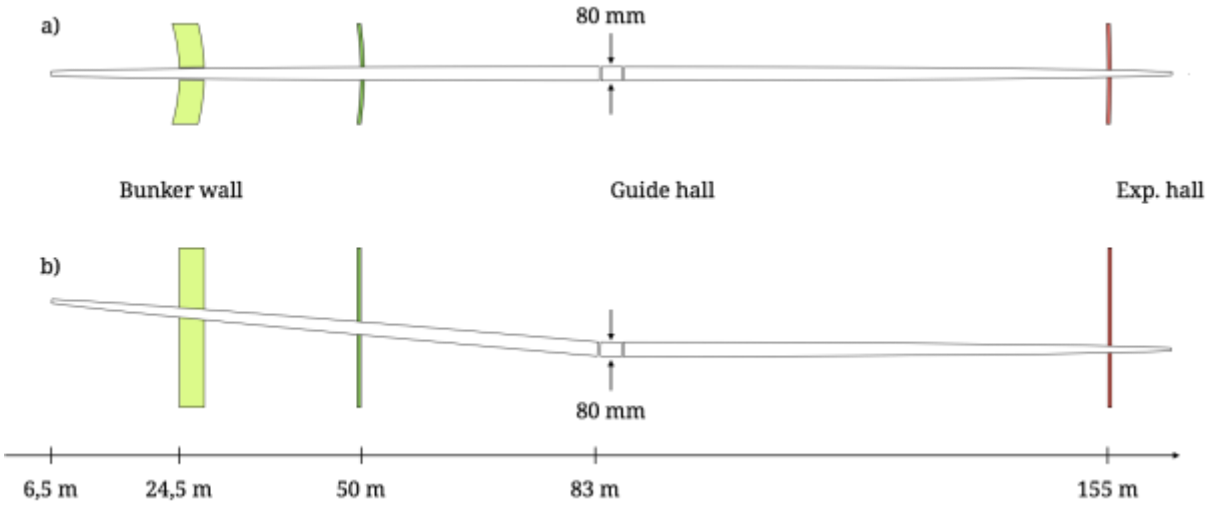

Figure 4.1.4.1: *a) top view of the elliptic guide system. b) Side view of the elliptic guide system.*

The horizontal design is a single straight ellipse starting at 6500 mm and ending at 157500-mm. This ellipse is divided in two 74000-mm half-ellipses connected by a 3000-mm straight guide element. A horizontal shift of 34 mm toward the thermal moderator will ensure maximum thermal Brilliance Transfer while keeping the complete guide system between the guide hall pillars. The ellipse parameters are: 2a = 158300 mm and 2b = 80 mm with an entry focal point at 5000 mm and an exit focal point at 2290 mm.
The vertical design is a single ellipse divided in two 74000 mm half-ellipses connected by a 3000 mm straight channeled guide element. The first half-ellipse is inclined by 0.46° to point at the Moderator. The straight part is tilted by a 0.23° with respect to the first ellipse (-0.23° in absolute). The total beamline declination is of -658 mm. The second half-ellipse is again tilted by a 0.23° angle with respect to the straight part (0° in absolute). The incident beam is therefore horizontal at sample position. The ellipse parameters are: 2a = 156230 mm and 2b = 80 mm with an entry focal point at 3700 mm and an exit focal point at 1530 mm.

During the optimization process, several guide geometries were investigated from a constant cross-section curved guide to a double elliptic design. With the additional constraint of transporting and polarizing thermal neutrons, our simulations showed that these alternative designs have either a dramatic negative impact on BT, polarization and/or cost.

4.1.4.2 m-coating

m-coating optimization have been carried out for each super-mirror using McStas by logging the position and critical angle of each reflection.

As the guide is a straight ellipse in the horizontal plane, the left and right mirrors will be coated with $1.5 < m < 4$ following a classical *m* distribution versus length.

In the vertical plane, the two kinks are inducing higher *m* coating on the straight element and the second half ellipse. The straight element will be coated with a fixed m=4 coating on the

reflective side (bottom mirrors) while the upper mirror will remain uncoated. For the second half-ellipse, neutrons will be bouncing between the top and bottom mirrors inducing higher *m*-values at specific locations. We will use the maximum value of (m_{top}, m_{bottom}) as the envelope in this area. The two half-ellipses will be coated with non-magnetic Ni-Ti while the polarizing straight section will be coated with FeSi.

The results of the optimization are presented on fig. 4.1.4.2.

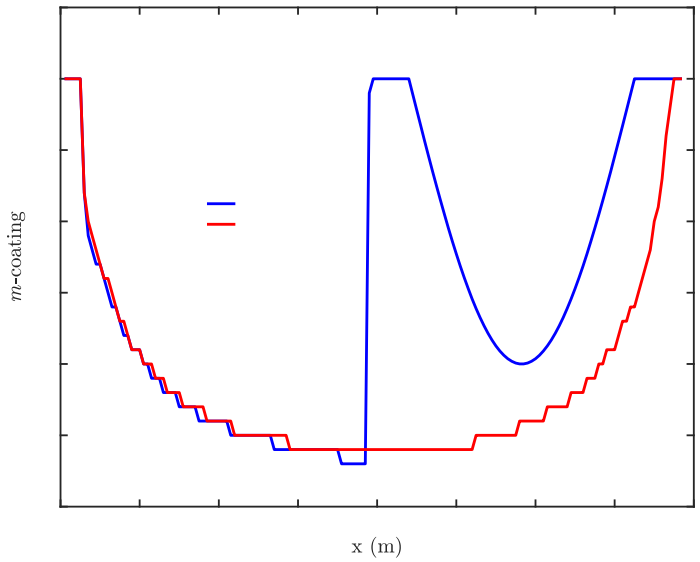

Figure 4.1.4.2: *optimized m-values for vertical and horizontal super-mirrors.*

4.1.4.3 Performance

Here we present the transport performance of the guide system for both the thermal and the cold spectra. The quality of the optics is defined by the brilliance transfer, the divergence profile and the beam shape over the whole wavelength range. A mean Brilliance transfer of 73% is achieved on the thermal spectrum and 76% on the cold spectrum. The beam shape and divergence are in excellent agreement with the FoM. The BT is decreasing on both spectra at large wavelength due to gravity, the beam center for cold neutrons being a few µm below beam center line.

The total thermal flux at sample position is of 4.75×10^9 n/s/cm^2 whereas the cold flux is of 3.25×10^9 n/s/cm^2 between 2 and 3.7Å and 1.20×10^9 n/s/cm^2 between 3.7 and 5.4 Å. These fluxes are unpolarized fluxes. Half of the flux will be lost with polarization.

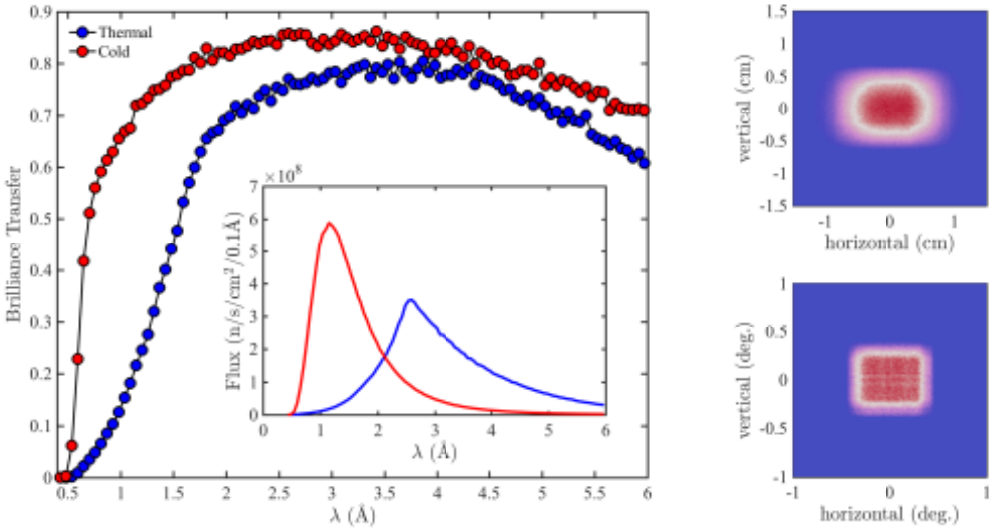

Figure 4.1.4.3: *(left) expected brilliance transfer from the neutron optics. The thermal spectrum is transported by the elliptic guide only while the cold spectrum make use of the additional SSB. Inset: expected flux at sample position. (Right) beam characteristics at sample position (top: shape, bottom: divergence).*

4.1.5 Beam geometry conditioning (13.6.18.1.4)

4.1.5.1 Collimation slits (13.6.18.1.4.2)

The MAGiC collimation slits system will be based on the DREAM one. A set of independent slits will be installed in the last meters of the neutron guide. Three possible collimations will be available to the users: +/- 0.3°, +/- 0.2° and +/- 0.1° in agreement with the System Requirements. We intend to use vacuum-proof piezo drives from the supplier SmarAct.

The slit positions are given by the distance xs to the sample position at 159000 mm:

Slit	xs (m)	y,z (mm) (guide)	y0,z0 (mm) (min.)	Translation (mm)
1	-2.00	8.0	5.7	2.3
2	-2.50	10.1	8.6	1.5
3	-3.00	11.1	5.1	6.0
4	-7.00	16.6	12.4	4.2

This will provide three optional divergences. It is preferable to have y and z-axis independent. For additional focusing, see below, all slits are open.

Resolution:

+/- 0.3° (FWHM) no Slits
+/- 0.2° (FWHM) using Slits 1 and 2
+/- 0.1° (FWHM) using Slits 1, 2, 3, 4

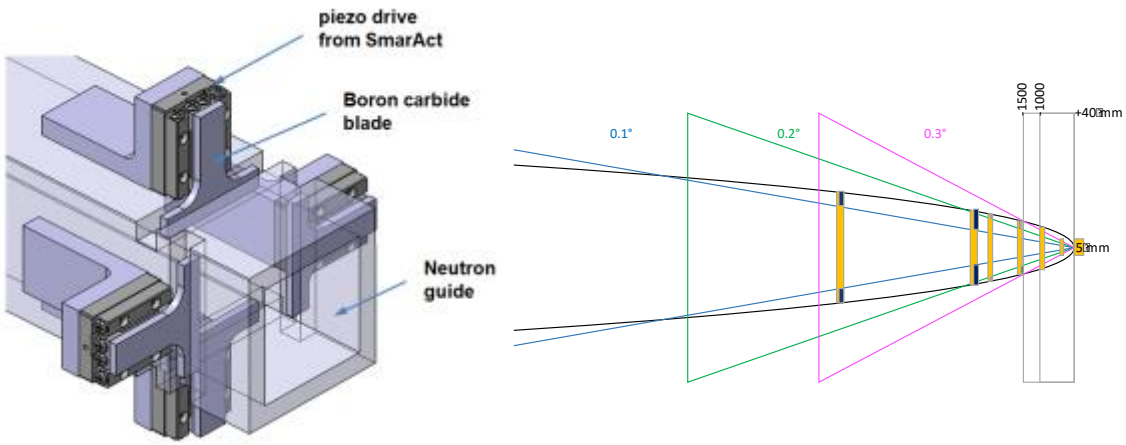

Figure 4.1.5.1: *schematic of the in-guide DREAM's collimation slits*

4.1.5.2 Focusing (13.6.18.1.4.1)

An optional focusing device can be installed at the elliptic guide exit to focus the beam on a 1x1 mm^2 area. The current design is a 1.1 m long elliptic nose coated with *m*=6 Ni-Ti. The calculated gain factor is 4 in terms of flux with an increased divergence of +/- 0.8° (theoretical gain: 7). Using a longer focusing device will naturally increase the flux up to a factor 9 for a 1.4 m device. The detailed design of this element will be defined by the radial collimators and sample environment characteristics during the detailed design phase.

4.1.5.3 Beam cleaning

A final 10 cm long boron carbide nose will be used to clean-up the beam before the SE. Multiple diameters will be available to perfectly match each incident beam and sample characteristics.

4.2 Choppers (13.6.18.1.3)

- The BTS shall transport a 1.7 A bandwidth from moderator to sample position in the 0.6-6 A range with a wavelength resolution in the 0.1 < δλ/λ < 1.2 % range at 6 A and 1 < δλ/λ < 12 % range at 0.6 A.
- The BTS shall tune the pulse width to transport a neutron beam with a wavelength resolution in the 0.1 < δλ/λ < 1.2 % range at 6 A and 1 < δλ/λ < 12 % range at 0.6 A.
- The BTS should be able to provide monochromatic sub-pulses at sample position.

In summary, the chopper system consists of

(i) two counter-rotating pulse shaping disc choppers (PSC) at 6.24 m,
beam width: 28.8 mm x 29.8 mm (WxH)
The **PSC** uses a disc diameter of d=60cm and operates usually below 200Hz. The chopper disc has a small opening of 4.5cm width for best resolution. A slit width of 4.5cm and counter-rotation with 112Hz and 112Hz yields 120 µs pulse width. With an additional 105° opening segment (opposite to the 4.5cm/8.6° slit) on both counter-

rotating discs, it is further possible to achieve a rather favorable wavelength-dependent pulse width. Here, the beam is opening within 60 µs, while closing is determined essentially by the end of the ESS pulse.

(ii) one 14Hz pulse selection disc chopper (SC) at 6.70 m for one wavelength frame only
beam width: 26.5 mm x 29.3 mm (WxH)
With a diameter of 60 cm, the opening and closing time is 1.1 ms. The required passage time for one pulse of the PSC is 3ms, including opening time of the beam cross-section of 1.1ms, results in one slit of 20.6° (4.1ms).

(iii) one 14Hz band control disc chopper (BC) at 80 m with a 180° window on a disc of 75cm diameter. The **BC** defines the wavelength band for the TOF frame at the detector position. The opening and closing time for the 80 mm beam width is 2.6 ms.

(iv) for upgrade consideration and space requirements
two Fermi chopper (FC) after the end of the neutron guide, which is 150 cm before the sample. Their purpose is to select a series of wavelengths for inelastic studies. The two **FCs** can be placed next to each other with 80mm distance of the rotor axes in a common housing of 205 mm length in beam direction and 125 mm width. The Fermi choppers can be moved out of the beam within their housing. The rotor concept can be adapted to the design of the small FC of the instrument TOPAS at MLZ.[1]

The interplay of the chopper system is illustrated in acceptance diagram (t, λ) below.
It is possible to tune the wavelength resolution in the $0.05 < \delta\lambda/\lambda < 1.2$ % range at 6 Å and $0.5 < \delta\lambda/\lambda < 12$ % range at 0.6 Å. Pulse width may optionally depend on λ.

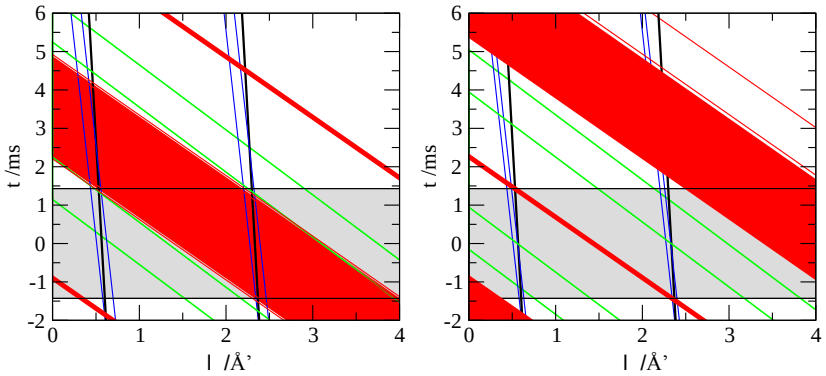

Figure 4.2: *(left) An example of wavelength dependent pulse shaping from 150µs at 0.6Å to 2.8ms at 2.3Å. (right) An example for high resolution mode of 120µs pulse width for all λ. (red: PSC, grey: ESS pulse, green: SC; blue: BC, black: detector TOF frame.)*

[1] The slit package consists of a Si-wafer stack covering a beam cross-section < 24×24mm^2. The two FC provide different resolution setting with large flexibility; in combination of both FC the repetition rate and resolution can be decoupled. The thickness of each wafer is d=280µm and 420µm for the first and second FC respectively. Both FC have a length of L=6.6mm. Operating at a frequency of 48×14Hz=672Hz, the maximal repetition rate is 96×14Hz, yielding a minimal pulse width of 20µs. The second FC selects various subsets out of the 96 sub-pulses defined by the first FC, by spinning at 1/2 (1/3, 1/4) of the first FC frequency and using a coarser collimation, with d=2×280µm. This combination allows for varying the time-resolution in steps of 20µs, 30µs, 40µs, and 60µs for a constant number of 48 TOF frames per pulse. For large wavelengths a smaller number of TOF frames can be chosen, for example 36 or 24 frames with additional options for relaxed resolution by either combinatorial selection or reduction of speed. The FC slit package is made of Si-wafers, which are separated by absorbing layers of thickness $d_{Å,}$ combining ~45µm Gd (best at E<150meV) and a top layer of ~85µm ^{10}B (more favorable γ spectrum and more efficient >150meV). Note, because of the inclined neutron path through the absorber, the effective total absorbing thickness is > $d_A L/2d$ ~ 0.76mm.

4.2.1 Chopper Pit 1: Pulse Shaping Chopper and 14 Hz Overlap Chopper

The pulse chopper and the overlap chopper are mounted together in one chopper pit.

PSC parameters:
Position: 6.24 m
Disc outer diameter d = 60 cm
Beam height: h = 29.8 mm
Frequency: <112 Hz
Slit opening: 105° and 8.6°
Phase accuracy: 0.15°
Disc material: carbon fiber
Absorber: 200mg ^{10}B /cm^2

SC parameters:
Position: 6.70 m
Disc outer diameter: d = 60 cm
Beam cross-section width: 26.5 mm
Beam height: h = 29.3 mm
Frequency: 14 Hz
Slit opening: , 20.6°
Phase accuracy: 0.3°
Disc material: Al-alloy
Absorber: 200mg ^{10}B /cm^2

4.2.1.1 Spindle units

The spindle units are magnet bearing systems as used in all FZJ high speed choppers.

4.2.1.2 Enclosures

The enclosure need to ensure the containment of all rotor fragments in case of rupture at high speed. Possible material candidates are mild steel or high performance aluminium alloys. Steel might need a Ni coating to ensure clean vacuum proof surfaces.

4.2.1.3 Vacuum

The choppers are operated under vacuum of $\leq 10^{-3}$ mbar.

4.2.1.4 Integration in guide system

Pulse chopper and selection chopper are connected by an evacuated flight tube. The assembly of pulse and selection chopper share their own atmosphere. There are neutron windows of 0.5 mm thick AlMg3 (to be confirmed by structural calculations) on the entrance to the pulse chopper and the exit of the selection chopper.

Due to the slope in the first part of the neutron guide the beam height for the overlap chopper is 4 mm less than for the pulse chopper. We will address this by locating the overlap disk 4 mm lower instead of tilting the complete chopper setup.

4.2.1.5 Chopper Extraction System

The Pulse Shaping and 14 Hz overlap choppers are rigidly integrated into one assembly. The complete assembly can be vertically extracted from their common socket by means of guiding elements reaching to the bottom of the bunker roof. The standard extraction system for double disk choppers in so called over/under configuration is currently developed together with the ESS chopper group. The same principle can be used for the MAGiC assembly of pulse and overlap chopper.

From the preliminary model of MIRACLES as provided by ESS we do not expect severe interferences since the MIRACLES choppers are located in a larger distance to the monolith than the MAGiC choppers. However, we have identified some interference between the socket of the MAGiC chopper with the first MIRACLES chopper. We expect that this can be cleared easily.

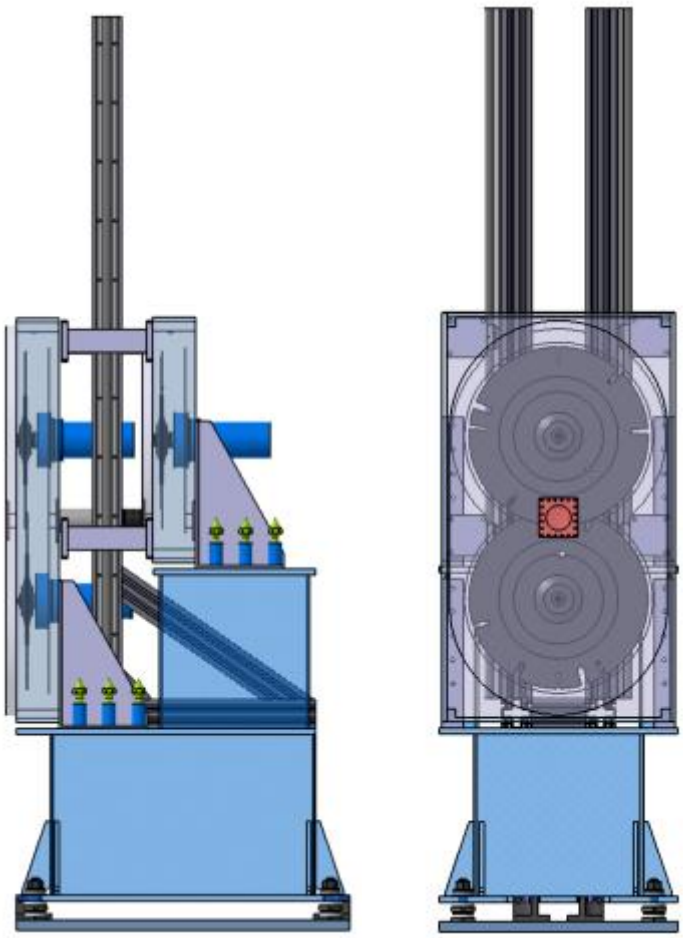

Figure 4.2.1.5: *Integrated chopper pit for pulse shaping – and selection chopper..*

4.2.2 Band Chopper

BC parameters: Position: 80 m
Disc outer diameter d = 75 cm
Beam height: h = 8.0 cm
Frequency: 14 Hz

Slit opening: 180°
Phase accuracy: 0.3°
Disc material: carbon fiber
Absorber: 200mg ^{10}B /cm^2

4.2.2.1 Spindle unit

The spindle unit is a magnet bearing system as used in all FZJ high speed choppers.

4.2.2.2 Enclosure

The enclosure needs to ensure the containment of all rotor fragments in case of rupture at high speed. Standard aluminium alloys are suitable due to the limited rotor speed. The enclosure is a horizontal split housing according to the endorsed ESS CHIM variant DC-SR common vacuum

4.2.2.3 Vacuum

The choppers are operated under vacuum of $\leq 10^{-3}$ mbar.

4.2.2.4 Integration in guide system

The horizontal split housing allows protruding neutron guides inside the lower part of the housing minimizing the gap between guide ends and chopper disc. The housing is connected to the guide vacuum tube by metal bellows and ISO vacuum connectors. The lower housing is installed together with the guide system on a solid base and adjusted. The upper part will be introduced vertically using guiding elements. The chosen polymer seal (O-ring) will be attached to the upper housing part and can be replaced during maintenance without entering the bunker. Connecting screws can be fixed from the (lower) bunker roof level with extended tools. The screws will be attached and secured to the upper housing.
Due to the slope of the MAGiC neutron guide the band chopper is located 642 mm below the ISCS origin at the moderator. For easier extraction, the chopper will not be tilted accordingly but placed vertically.

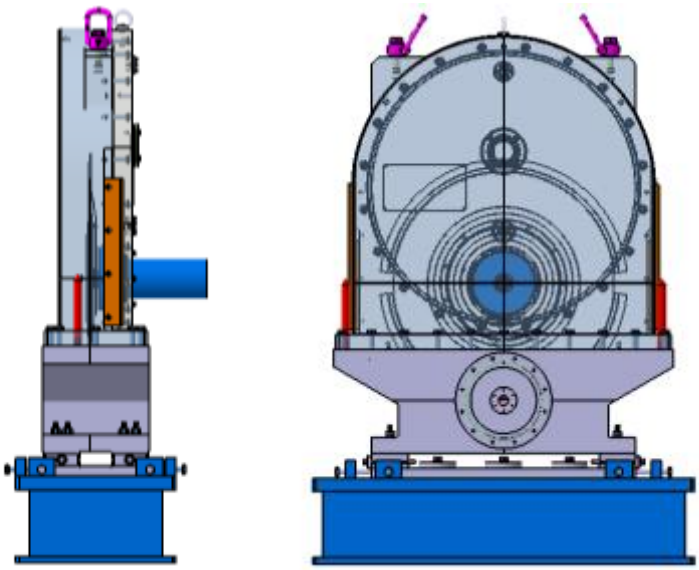

Figure 4.2.2.4: *Band control chopper (BC) pit with vertical spit housing.*

4.2.3 Mode of operation

Parking position of choppers is open. Sequence for starting the choppers to operation is in principle arbitrary.

4.2.4 Failures

Pulse shaping chopper failure: If one of the two is still operational, it is still possible to work at relaxed time resolution > 240µs. If both PSC are not operational, low resolution with ESS pulse width is still possible.
14 Hz Overlap chopper failure: this may lead to spurious contaminations depending on the chopper phases.
Band control chopper failure: Note that the projection of the pulse shaping chopper on the source pulse already defines the two wavelength bands. The purpose of this band control chopper is actually a precise termination at the short wavelength end of each of the two bands and suppression of the afterglow for shorter wavelengths than used. Upon BC failure, the chopper system is still functional, however, TOF-frame overlap needs to be excluded within the data reduction, and additional background will arise.

4.2.5 Chopper Control System

The MAGiC chopper control system will be designed in accordance with the standard ESS control system. This includes one CHIC system for each rack and individual drives for each axis. All components will meet the design guidelines in the ESS chopper handbook.
Every control rack is a standalone unit with no hardware communication connection between the different chopper drives. A control rack fits into the ICS as shown in Figure 4.2.5.

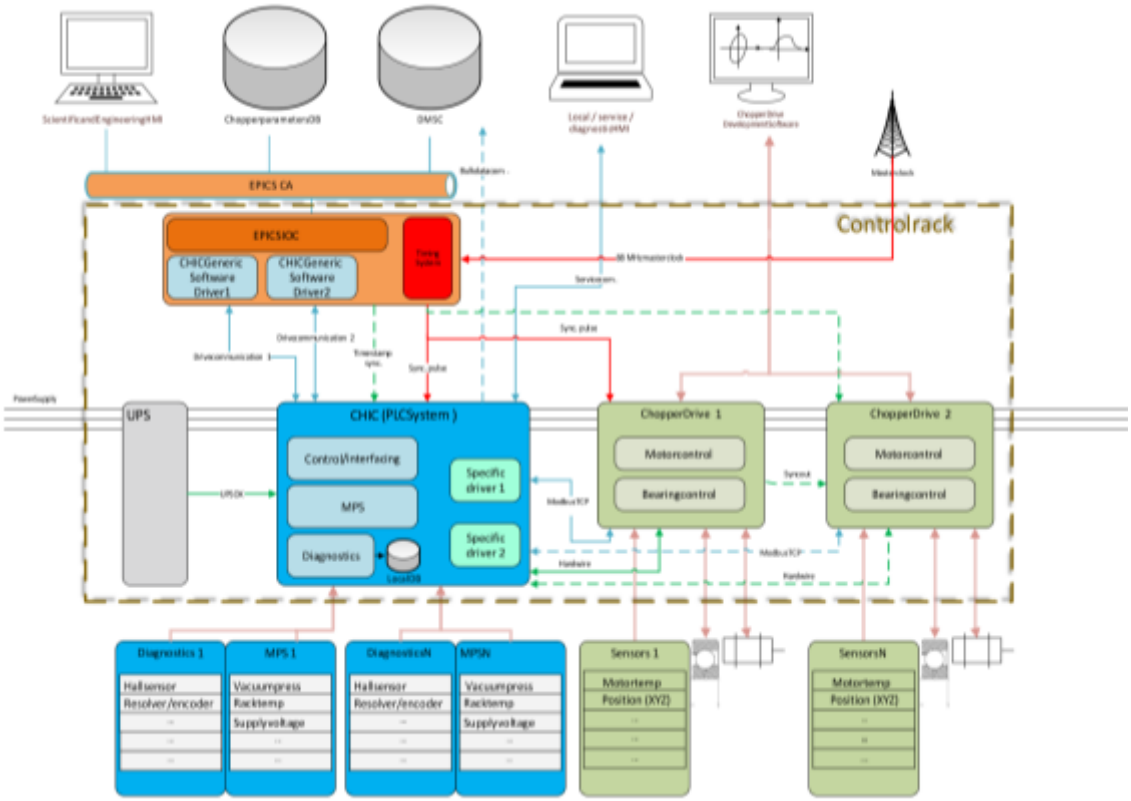

Figure 4.2.5: *Integration of the chopper control system.*

4.3 Polarization (13.6.18.1.5 & 13.6.18.3.1)

4.3.1 Thermal neutron polarization

The instrument shall provide a polarized thermal beam with a mean polarization rate of <P>=97%.

Thermal neutrons polarization will be achieved by the 3 m long channeled guide element connecting the two half-ellipses. The 0.23° kink will force a polarizing reflection for wavelength up to 3.5 Å. Its cross-section is of 80x80 mm divided horizontally into 6 identical channels using 300 μm Si wafers. Each channel is 80x13 mm (WxH) corresponding to an angular aperture of +/- 0.24°.

It is positioned at x=80500 mm in the middle of the elliptic guide. At this specific position, the transported neutron beam has the lowest divergence, ensuring that each neutron will be reflected on the bottom super-mirrors. Best performance is obtained when a 1 kG magnetic saturation field is applied on the supermirrors. Strong and homogeneous magnetic field is created by $Nd_2Fe_{14}B$ (N42, B_R=1.28T) magnets placed inside of a soft iron yoke.

Our McStas calculations were carried out using a m=4 coating for the reflected spin state and a m=0.7 coating for the transmitted spin state. The expected polarization on the thermal spectra is reported in figure 4.3.2. The mean polarization for $0.7 < \lambda < 2.3$Å is 99%. Looking at the polarization profile one can see that the polarization rate starts to deteriorate for $\lambda > 1.8$ Å. This behavior is inherent to FeSi coating for which low angle reflections (up to m=0.65) are are identical for both spin states. However, 90% polarization rate at 2.5Å is still sufficient for most of the planned experiments.

4.3.2 Cold neutron polarization (13.6.18.1.5.4)

The instrument shall provide a polarized cold beam with a mean polarization rate of <P>=97%.

To polarize cold neutrons over the complete wavelength band while ensuring a good BT, one can reflect neutrons on FeSi super-mirrors from silicon. The refraction index of silicon eliminates the low angle non-polarizing part of the FeSi reflectivity curves with the cost to pay being the silicon absorption (see fig. 4.3.1.2).

On MAGiC, we will make use of the SSB to polarize the cold spectrum. The bender assembly will be inserted in a vertical magnetic field to saturate the FeSi supermirrors. Strong and homogeneous magnetic field is created by $Nd_2Fe_{14}B$ (N42, B_R=1.28T) magnets placed inside of a soft iron yoke (see fig.4.1.3.1). External dimensions of the yoke are 80x70x100mm (WxDxH) with a soft iron thickness of 10 mm. COMSOL calculations showed a magnetic field of at least 1 kG over the whole SSB volume, which is sufficient to

saturate supermirrors. Two additional magnets on the internal sides are used to homogenize and increase field at the center of the bender.

Our McStas simulations were carried out using a *m*=3.2 coating for the reflected spin component and a residual *m*=0.1 for the transmitted component. A mean polarization rate of 99.5% is achieved by the SSB with a small decrease at large wavelength. The results are presented in figure 4.3.2.

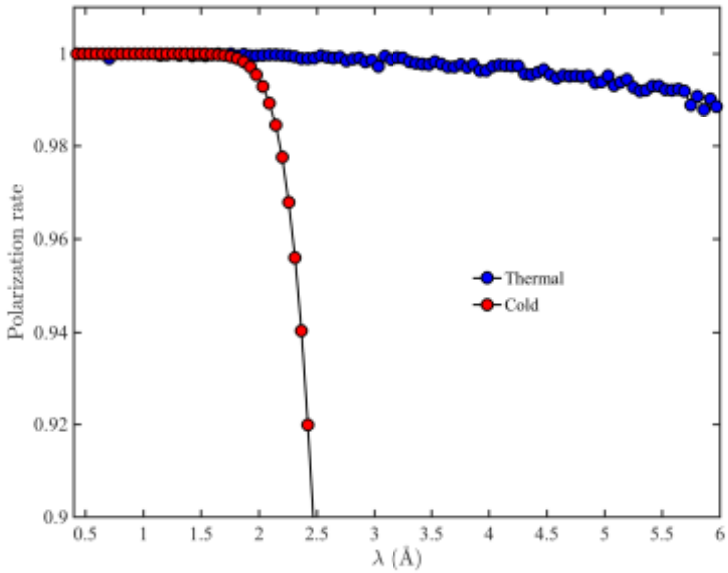

Figure 4.3.2: *expected polarization for the thermal (red) and cold spectra (blue) at sample position.*

4.3.3 Polarization analysis

- The BTS shall provide analysis of the scattered neutrons spin state for neutrons of wavelength > 2 Å over a wide angle (120°x6°).
- The BTS shall provide a way to perform XYZ polarization at sample position for neutrons of wavelength > 2 Å.

4.3.3.1 Polarization Analyzer (13.6.18.3.1)

Polarization analysis for cold neutron (2 - 6 Å) will be permanently installed on the instrument. The analyzer is based on the solid-state technology used for the SSB. 150 µm thick silicon wafers will be coated with FeSi and stacked in an inclined geometry. Each wafer will be 0.15x33x120 mm (WxDxH) with a *m*=3.2 coating corresponding to a 0.64° acceptance at 2 Å and perfectly matching the beam divergence. The wafers will be coated under strain, inducing a remanent magnetization. After magnetization (will be done at PSI), a holding field of 100 G will be sufficient to maintain FeSi magnetization over time. In test measurements, we investigated FeSi polarizers with m=3.2 coating with a holding field of only 45 G (see figure 4.3.3.1). A polarization of about 95 % was observed.

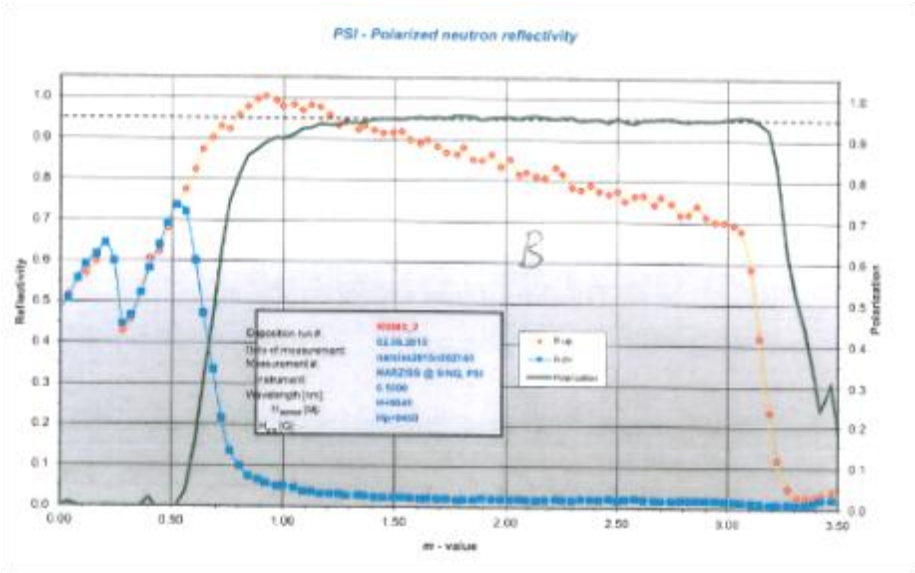

Figure 4.3.3.1: *Developed FeSi polarizer for MAGiC*

To limit the effect of stray field from SE on the analyzer, the super-mirrors magnetization will be aligned with the vertical stray field of the superconducting magnet. Extra care will have to be taken to minimize the resulting forces on the saturating magnets. The superconducting magnet will be provided by ESS through the SAD. The detailed design of the saturating field can only be made after a proper stray field calculation.

The analyzer will cover 120° x 6° (0.2 sr) on a 900-mm radius, corresponding to 12566 blades to coat and assemble. The analyzer is the critical path for the delivery (the production of the 12566 polarizers will take around 2 years) of the instrument into user operation. Its delivery is scheduled for Q1 2022, therefore, hot commissioning, will start without the polarization analysis capabilities.

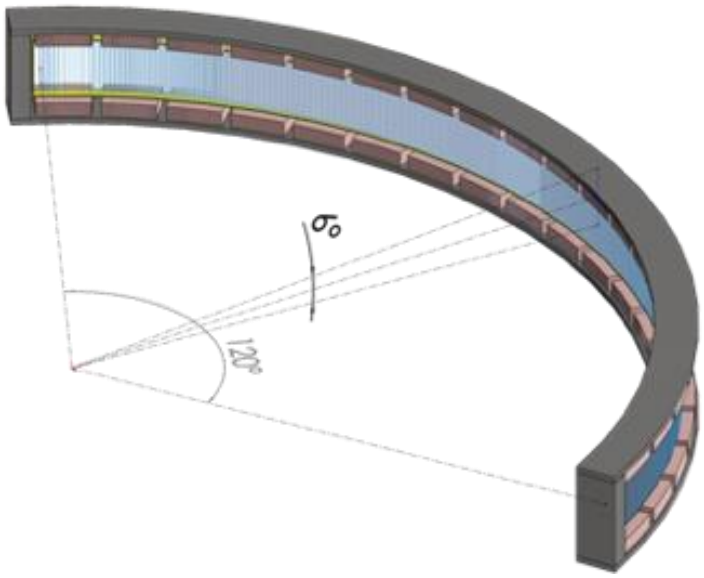

Figure 4.3.3.2: *simplified layout of the polarization analyzer.*

4.3.3.2 XYZ analysis (13.6.18.1.5.3)

For XYZ polarization analysis the neutron polarization needs to be turned adiabatically into +/- X, Y, Z direction at the sample position and back to the accepted polarization direction Z of the analyzer. Therefore, we consider three elements

(i) two (DHD) Double-Helix-Dipole[2] coil sets in the initial neutron path for turning guide field and polarization,

(ii) a modified PASTIS setup[3], which provides homogeneous magnetic field near the sample,

(iii) a radial coil set in front of the analyzer with compensation at the sample position for adiabatic field change into the vertical field near the analyzer.

The magnetic fields and hence the functionality of these elements do not strongly interfere with each other. The DHD coils can be thought of consisting of pairs of slanted current sheets (at 45° inclination) wound on a cylinder with an axial rotation of 180 degrees. The coils generate a highly homogeneous field, and depending of polarity and current, it changes continuously from a solenoidal to any transverse field. The DHD coils provide a convenient tool for achieving field changes into arbitrary direction for neutrons with wavelengths down to 0.6 Å.

The PASTIS setup has been developed originally to provide an extremely homogenous field distribution for using He-3 polarization analysis. Here, we use it under relaxed requirements with benefitting from the open view in the scattering plane. The setup is modified here by avoiding vertical bars at the corners of the ferrite plates. Furthermore, by shifting the sample position to a level at one third of height, there is an open view to the full large detector.

The radial coil set, including an outer coil for compensation of the field at the sample position, is designed for adiabatic field change for 2 Å neutrons from the sample to the analyzer. The coil set is wired on an Al-housing, which is filled with Ar and has absorbing walls to reduce background.

The figure 4.3.3.2 shows the current conceptual design with a suitable geometry, however, the field configurations are still to be optimized in the detailed design phase.

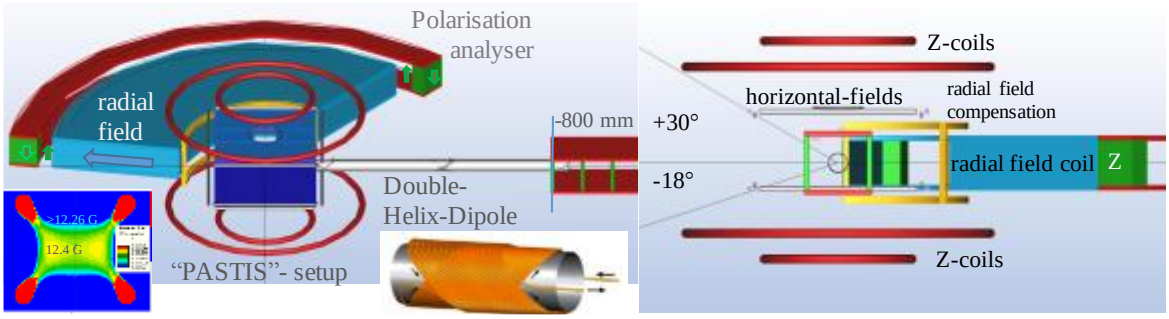

Figure 4.3.3.2: *(left) magnetic field homogeneity at sample position. (right) coil arrangement.*

[2] P J Masson et al., Proc COMSOL 2010; H Soltner et al., Proc PAC07 2007.

[3] J Voigt et al., EPJ Conf. **83**, p0316, 2015*; https://arxiv.org/pdf/1201.5208*;

4.3.4 Spin handling

4.3.4.1 Guide magnetic field (13.6.18.1.5.1)

To guide neutron polarization without losses to the sample position the appropriative magnetic field along all the neutron path should be applied. The configuration, strength and homogeneity of the field are defined by the neutron wavelength, neutron beam cross-section and possible perturbations in the neutron beam path like choppers, collimation systems, neutron guide joints et cetera. We proposed to use well known guide magnetic system consisting of two parallel soft iron plates connected by permanent magnets in such a way that most of stray fields from the poles of magnet loop are enclosed between these two plates Fig. *4.3.4.1.1*

The main parameters of the magnetic system (width and thickness of the plates, distance between plates, strength of the permanent magnets, number of the magnets per length, *Fig. 4.3.4.1.1*) defining the guide field were obtained by Comsol [https://www.comsol.com/] calculations. The strength of the guide field needed for the shortest neutron wavelength 0.6 Å is about 60 Gauss. This value was chosen to ensure "adiabatic" transition neutron polarization through all the neutron path including possible perturbations of the magnetic field. The NdFeB (N42) magnets with cross section 10x10mm and height 120mm can be used to get 60 Gauss (*Fig. 4.3.4.1.2.*) field in the volume corresponding maximal neutron guide cross section. 20 magnets are necessary for each 2m long guide section. The orientation of the guide field is vertical. Additional details can be found in the "*Spin Handling*" Additional File.

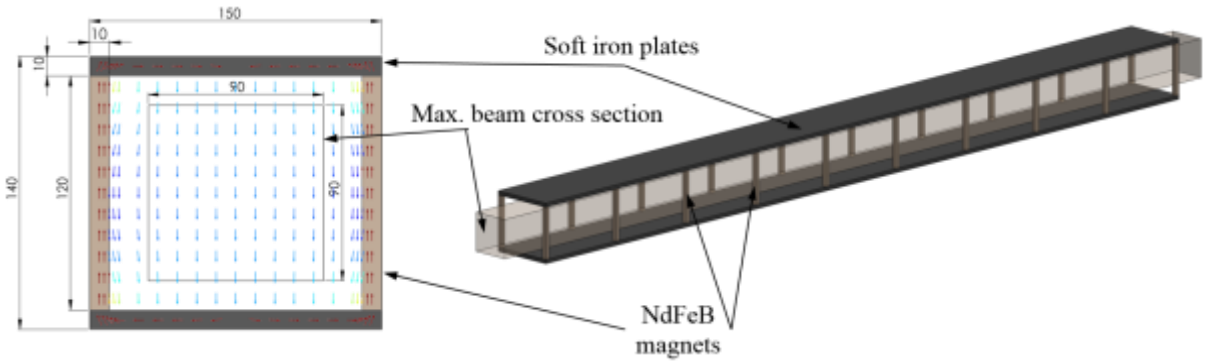

Fig. 4.3.4.1.1: *The magnetic system of the magnetic guide for MAGiC.*

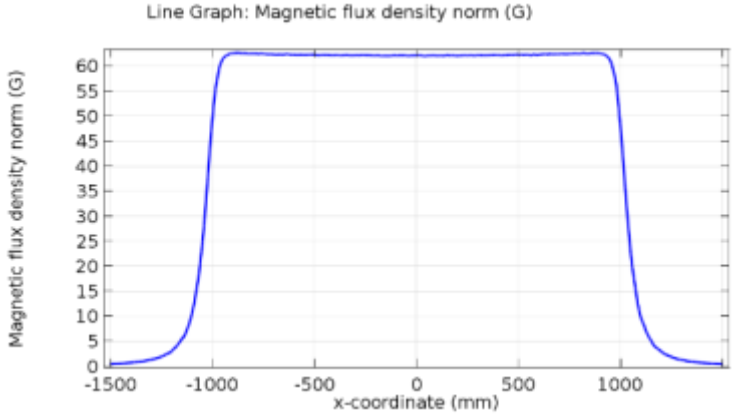

Fig. 4.3.4.1.2: *The calculated value of the magnetic field in the center of the neutron guide.*

4.3.4.2 Rotators (13.6.18.1.5.2)

The direction of the polarization after the solid-state bender and in the elliptic sections, is vertical. The orientation of the saturation field in the thermal neutron polarizer is horizontal due to horizontal orientation of the super-mirrors (vertical kink) Fig.4.3.3.2. Hence it is necessary to rotate polarization from vertical to horizontal direction at the thermal polarizer entrance. The opposite rotation will be done at the polarizer exit to match the polarization direction with the superconducting magnet stray field.

Each rotator consists of two pairs of NdFeB (N42) magnets placed inside of a soft iron yoke. The orientation of the magnetic field created by a pair of magnet is perpendicular to the field orientation of the second pair. Between the pairs, the magnetic field rotates by 90°. This rotation should be "adiabatic" with respect to the Larmor precession as described in the previous section. The final parameters of the rotators will be defined during detailed design of MAGiC.

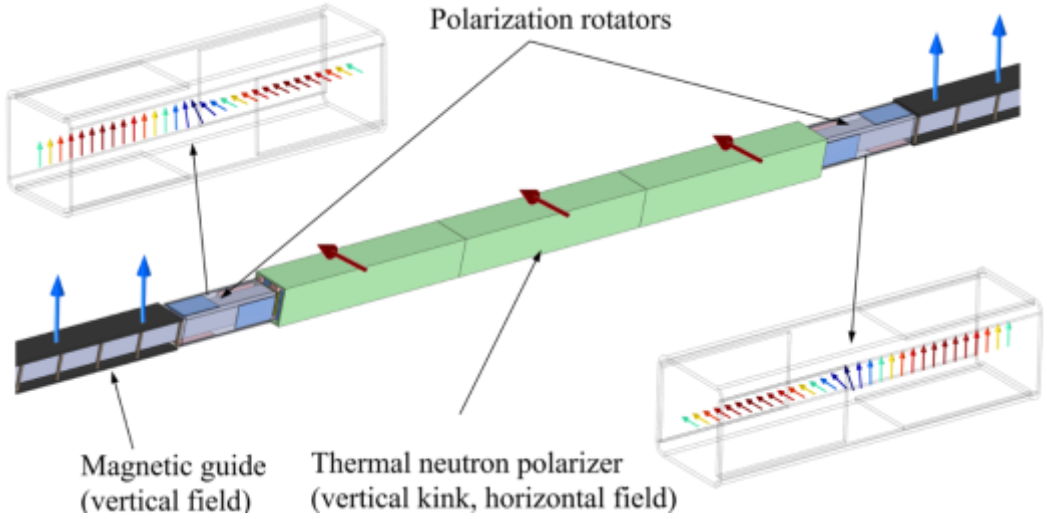

Fig.4.3.4.2 *Rotators turn polarization from vertical to horizontal direction at the polarizer entrance and turn it back to vertical at the exit.*

4.3.4.3 Spin flipper (13.6.18.1.5.1.5)

The BTS shall flip the incident neutron spin state with an efficiency of 99% over the whole wavelength range.

As a polarized instrument, MAGiC will be equipped with a RF adiabatic spin flipper. The spin flipper for MAGiC is composed of a solenoidal coil producing the oscillating radio-frequency field, a guide gradient magnetic field and a RF generator with amplifier (Fig *4.3.4.3).* Additional details can be found in the "*Spin Handling*" Additional File.

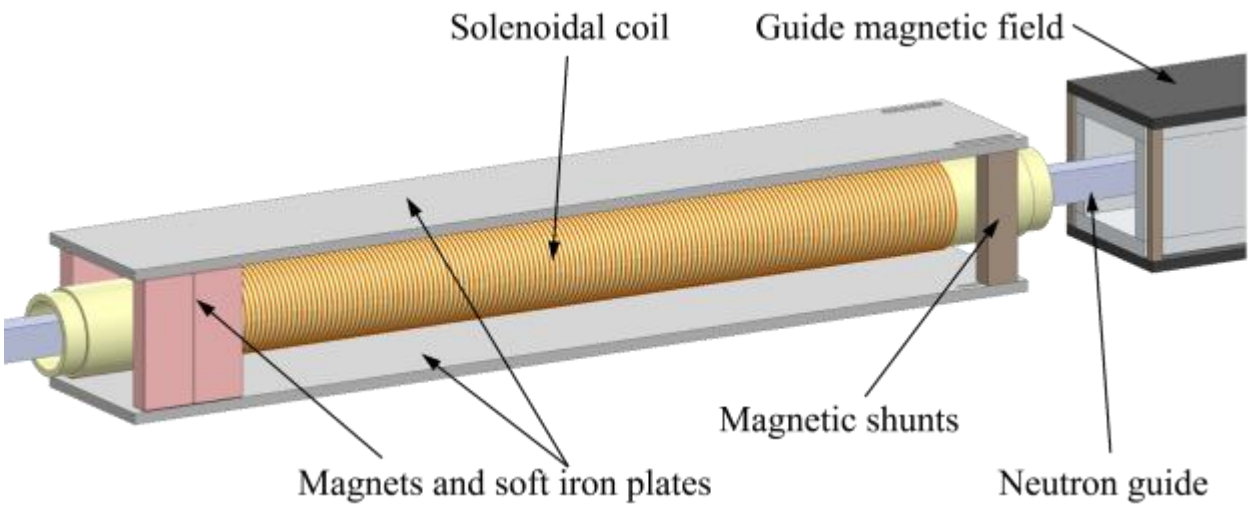

Fig 4.3.4.3: *draft of the adiabatic spin-flipper. Horizontal oscillating field is generated by the RF solenoid placed inside of the gradient filed assembly. Two soft iron plates, magnets and magnetic shunts create a vertical field with gradient along the neutron beam. The neutron guide is inserted inside of the solenoid.*

5 Sample Exposure and Characterization System

5.1 Sample Environment (13.6.18.2.3)

MAGiC will be a high throughput, polarized single crystal diffractometer capable of very fast measurements. In order to accommodate a large number of experiments and facilitate fast sample environment equipment (SEE) turnaround, the guidelines provided by SAD must be closely followed during design and construction phases. The checklist from SAD is attached to this document.

5.1.1 Dimensions

Around sample position, an 800-mm diameter free sample space has been reserved to accommodate for any sample environment equipment (up to XL type according to the SAD definition). The XL type SEE can be installed inside the cave using the instrument crane. The height of entrance doors to the cave is 3 m, allowing the separate delivery of the box and cylinder components, without removing the roof.

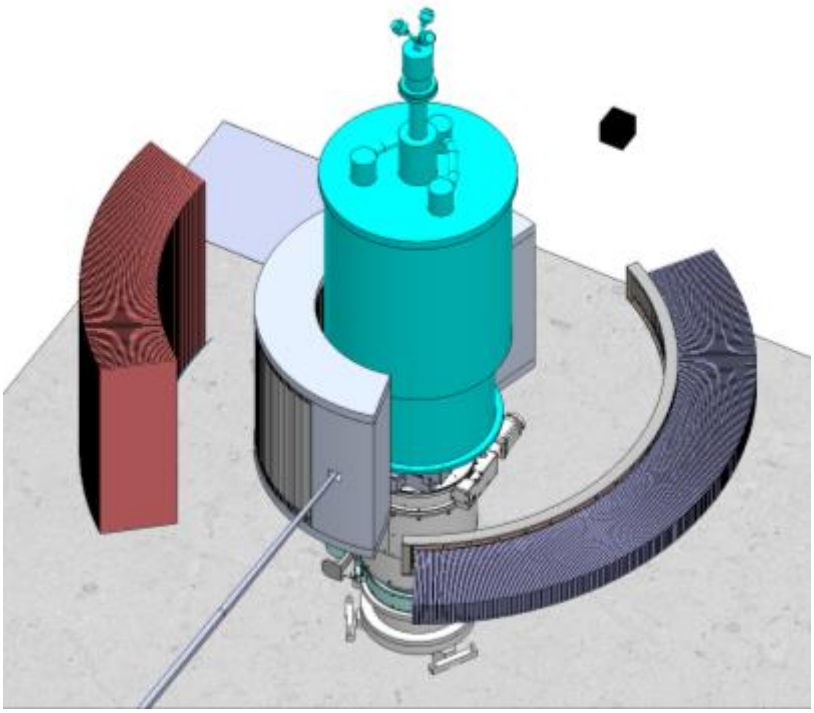

Figure 5.1.1: *aerial view of the sample space surrounded by the radial collimator and the two detectors. The sample space diameter is of 800 mm and occupied by a superconducting magnet.*

5.1.2 Devices

MAGiC will be initially equipped with a dedicated 1.5K wet cryostat. During user operations, MAGiC will also be equipped with a vertical split-pair superconducting magnet and a dilution fridge through the ESS SE pool.
The dedicated cryostat will be available during cold commissioning of the instrument. The current plan is to have an access to the pool equipment at the same time for integration purpose It will allow the first test experiments to be carried out at low temperature and/or under magnetic field during hot commissioning.

A dedicated setup of XY piezo-table and piezo-goniometer from attoCube will allow proper sample positioning inside any SEE. This setup has to be dilution and high magnetic field compatible. The sample table can be limited to a vertical translation (Z), two in-plane translation (XY) and one rotation around the vertical axis.

We are currently investigating the purchase of a 3D scanner and a 3D printer to tailor a specific sample holder for each sample.

5.2 Radial collimator (13.6.18.3.4)

The instrument should maximise the signal-to-background (S/B) ratio.

MAGiC will be dedicated to the study of complex magnetic samples for which signal/noise ratio has to be maximized. Most of the background on MAGiC will come from the sample environment as the beam has to go through multiple aluminum screens in the vicinity of the sample. Each screen will scatter parts of the incident beam to the detectors.

The best way to remove background from SE on the detectors is to make use of a radial collimator with its center being located at sample position. On MAGiC we will use a radial collimator in front of the large detector, and matching the angular aperture of the full scope detector configuration as upgrades will not be possible.

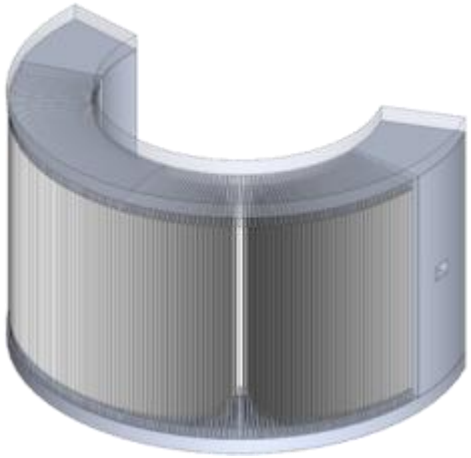

Angular spacing: 1.3°
Collimator angular span: 160° (120°)
Foil inside radius: 400 mm
Foil outside radius: 624 mm
Beam height: 624 mm (110mm)
Overall height: 624 < h < 1000 mm
Foil material: Mylar 36 µm
Absorber material: Gd_2O_3 2x25 µm

Figure 4.1.5.3: *large radial collimator design and characteristics.*

5.3 Detectors (13.6.18.2.3.2)

(see also Zusammenfassung MAGiC Detektoren 21.12.2016 in additional documents)

There will be two detectors, left and right to the beam axis, at 1m from the sample. One of these will be a large detector – **Detector A** – with 60° horizontal and +30° and -18° vertical acceptance. The detector will be upgradable to ~160° horizontal acceptance. The large solid angle is particularly important for the applied Laue method and is also adapted to the expected opening of an asymmetric vertical magnet of 8 to 10 T from the ESS SE-pool. The second detector – **Detector B** – has a 120° horizontal and a smaller +/-3° vertical acceptance with 0.2 sr solid angle coverage, which adapts to the geometry of the supermirror polarization analyzer. The required spatial resolution for both detectors should be 6 mm or better.

The preferred option for both detectors A and B is a ^{10}B based volume detector with inclined geometry of the Jalousie detector concept similar to the DREAM proposal. A prototype has been built and successfully tested for POWTEX at MLZ. This detector has a 3D grid of detection cells, working in coincidence mode of anode and cathode signals, rather insensitive to γ-background. The cathode layers are coated with 1 µm ^{10}B and are set in inclined geometry (η=10°), where several absorbing layers yield a measured detection efficiency larger than 50% at 1 Å.
There are favorable features of this volume detector: the distribution of counts into the detector's depth yields higher count rate capabilities. Furthermore, the resolution can be appropriately chosen to <6 mm (FWHM), and the surface projection of the 3D cells provides even an effective finer pixel mesh compared to the (FWHM) spatial resolution. Finally, the concept offers new possibilities to discriminate background from sample environment by the intrinsic collimation.
Here, for the design of the MAGiC detector, we have chosen a different arrangement of the detector modules positioned in a vertical cylinder geometry at 1m distance around the sample position. Another new feature is the single side coating with B-10 for improved resolution, which leads to a relatively large detection depth of 52 cm.

Finally, for an instrument upgrade consideration, an additional detector – **Detector C** –, could be placed underneath the sample environment to collect Bragg peaks. One possible option is a Cascade-type detector (CASCADE-M 2D-200, CDT, see additional documents) with 20x20 cm^2 detection sensitive area, with an expected spatial resolution is 2.5 mmx2.5 mm. With this resolution, the detector could be placed approximately 60 cm underneath the sample. One may note that in this geometry, the stray-field of a vertical magnet is not prohibiting the application of this detector type. This device is mentioned here for space consideration, and to explore the possibility of having a scattering window in the bottom of a vertical magnet. The efficiency (20% at 1Å) is lower than for the main detectors A and B, however, there is a significant value in collecting at least a part of the stronger out-of diffraction peaks.

5.3.1 Efficiency

The current specification aims at high efficiencies with 10 absorbing layers in inclined geometry for both detectors A and B, which are shown in the figure below.

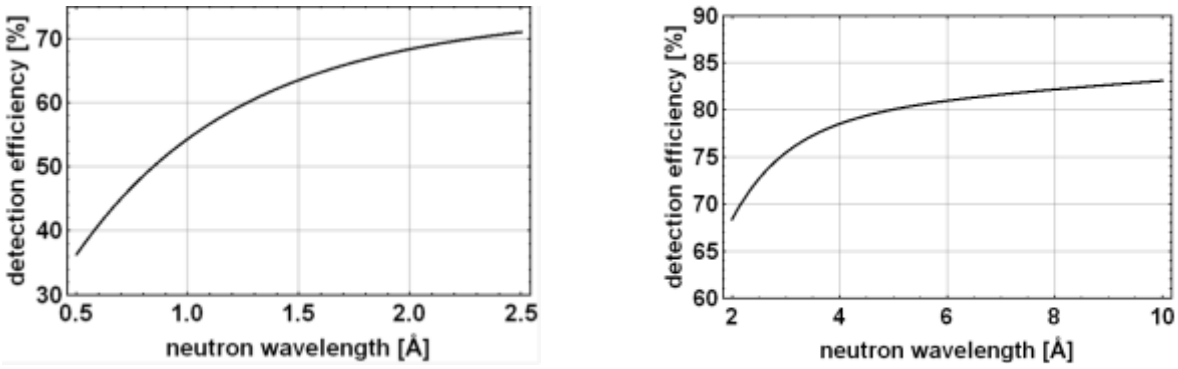

Figure 5.3.1: *Calculated effective detection efficiencies (left) of the proposed large MAGiC* ***Detector A*** *for thermal neutrons, >0.6Å (right) of the proposed small MAGiC* ***Detector B*** *for neutron wavelength > 2Å. Efficiency losses due to scattering from Aluminum structural material (housing, cathodes and converter substrates) are included in the model.*

5.3.2 Resolution

With single side coating it is possible to improve significantly the resolution perpendicular to the modules. In the design the best spatial resolution will be in 2theta direction 1.9 mm (FWHM), while in phi direction 5.6mm (FWHM) can be achieved.
Time resolution is determined by the flight path uncertainty given by the wire distances of 11 mm, which leads to ~10µs for neutrons of 4Å wavelength.

Large MAGiC detector A

Coordinate φ (vertical):

Number of channels in φ along the segment: 128
Width of channel (binning) $\Delta\varphi = 48°/128 = 0.358°$
Resolution in φ: 0.32° FWHM or 5.6mm FWHM at φ=90°

Coordinate 2θ (horizontal):

The volume along anode wires is divided through anode wires into 32 voxels of 16.7 mm length along the cathode strip. The projection of the coating in each voxel onto the entrance window gives the binning in 2θ.
$\Delta 2\theta_{cart}$ = 2.9 mm, $\Delta 2\theta = \arctan(2.9/1000) = 0.166°$
Resolution in 2θ: 0.12° FWHM or 2.1 mm FWHM

Depth:

Number of readout channels in depth: 32
Resolution in depth: 11.8mm FWHM

Small MAGiC detector B

Coordinate φ (vertical):

Number of channels in φ: 16

Width of channel (binning) $\Delta\varphi = 4.724°/16 = 0.358°$

Resolution in φ: 0.311° FWHM or 5.43mm FWHM at φ=90°

Coordinate 2θ (horizontal):

The volume along anode wires is divided through cathode strips into 32 voxels of 15,63 mm length along the anode wire. The projection of the coating in each voxel onto the entrance window gives the binning in 2θ.

$\Delta 2\theta_{cart} = 2.71$ mm, $\Delta 2\theta = \arctan(2.71/1000) = 0.156°$

Resolution in 2θ: 0.108° FWHM or 1.89 mm FWHM

Depth:

Total depth of the active detector volume along converter planes: 500mm.

Number of readout channels: 32, each 15.63 mm along anode wire, 15.39 mm along neutron path.

Resolution in depth: 11.0 mm FWHM

Electronics: For each SUMO there are 128 channels for anodes and 128 channels for cathodes, 1 CDRS-Board.

5.3.3 Fallback option

The fallback option for the detector system will be based on existing, standard He-3 technology either by assembling 8mm tubes or by using 2D position sensitive detectors to cover the scattering geometry in a similar way.

For single crystal Laue diffraction, the resolution is almost comparably good, however, the count rate capability of conventional He-3 detectors is lower by more than one order of magnitude compared to the baseline choice, and will impose limitations for applications to only very small single crystals.

5.4 Monitors (13.6.18.1.6)

There will be two monitors, before and after sample position, allowing to characterize the incident beam and the transmitted beam.

The characteristic of the monitors should be the following:

- 30x30 mm^2
- Pixel size: < 1x1 mm^2
- Time resolution: 1 μs
- Efficiency: 10^{-3}

A working solution could be based on the Micromegas Detector technology developed by CEA for the nTOF instrument at CERN [*Nuclear Inst. and Methods in Phys. Res. A* ***376****, 29-35 (1996)*]. Recent development showed that the technology is mature for low efficiency neutron beam profiling. This technology has been proposed as a possible standard for neutron beam loss monitor at ESS (2013).

6 Experimental cave (13.6.18.5)

6.1 Geometry

The experimental cave is a massive concrete structure assembled mainly from standard concrete (density = 2.4 g/cm^3) (see fig. 6.1.1 and 6.1.2). Its footprint on the floor is of 14.40 x 12.10 m^2. Its height will be 6 m internally to allow easy handling of the superconducting magnet sample cane. The cave base level is 60 cm above the experimental hall floor. Access by users and beamline staff will be made possible by stairs inside the cave. The side back access to the cave will be 4 m high and 2 m wide allowing easy handling of complex sample environment. A sliding door in the back wall (1.5 x 3 m) covered with boron carbide layer will ensure not direct line of sight inside the cave. Access to the corridor will be protected by an interlocked metallic fence. Inside the cave a free space will allow transfer of sample environment to sample position using the 1T hook. Around the detectors, free space of 1.5 m will be used for detector maintenance. Along the direct beam, this space will be used for the concrete/lead/boron carbide beamstop.

Future upgrades and installation may need an opening of the roof; therefore, a simple solution will be developed to ensure easy access to the cave using the experimental hall main crane. As for the walls, the roof will be assembled from standard concrete, its structure being ensured by steel rods.

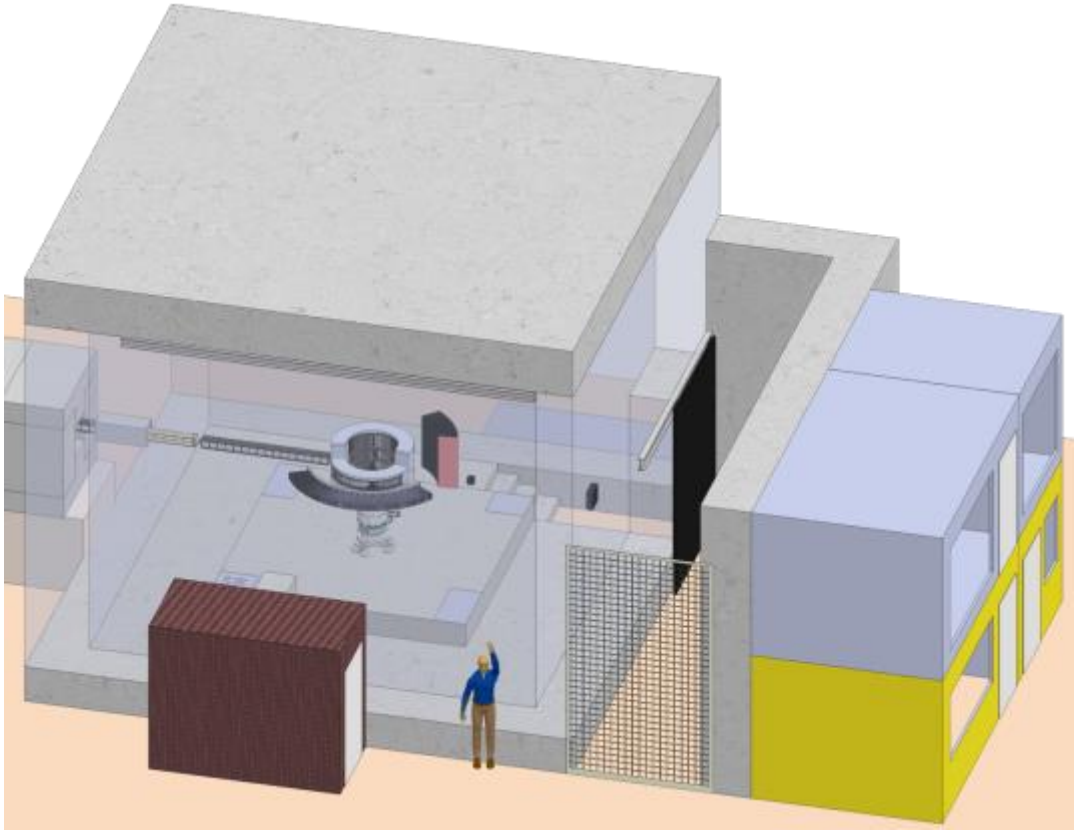

Figure 6.1.1: *3D drawing of experimental cave*

Two areas of 0.6 x 0.6 m and two areas of 1x0.5 m are reserved for auxiliary equipment as requested by the SAD group.

We reserve an area of 2 x 4 m^2 for the SEE preparation outside of the experimental cave. A visual pre-alignment of samples, cooling to the base temperature and adjustment of SEE parameters, will be done "off-line" in this dedicated area without logistic conflicts between user groups.

An additional area of 7 x 3 m^2 will be reserved for the control hutch and the sample preparation lab and a 3x1.5 m^2 one will be reserved for the computer towers and racks on the side of the cave, close to the instrument gallery.

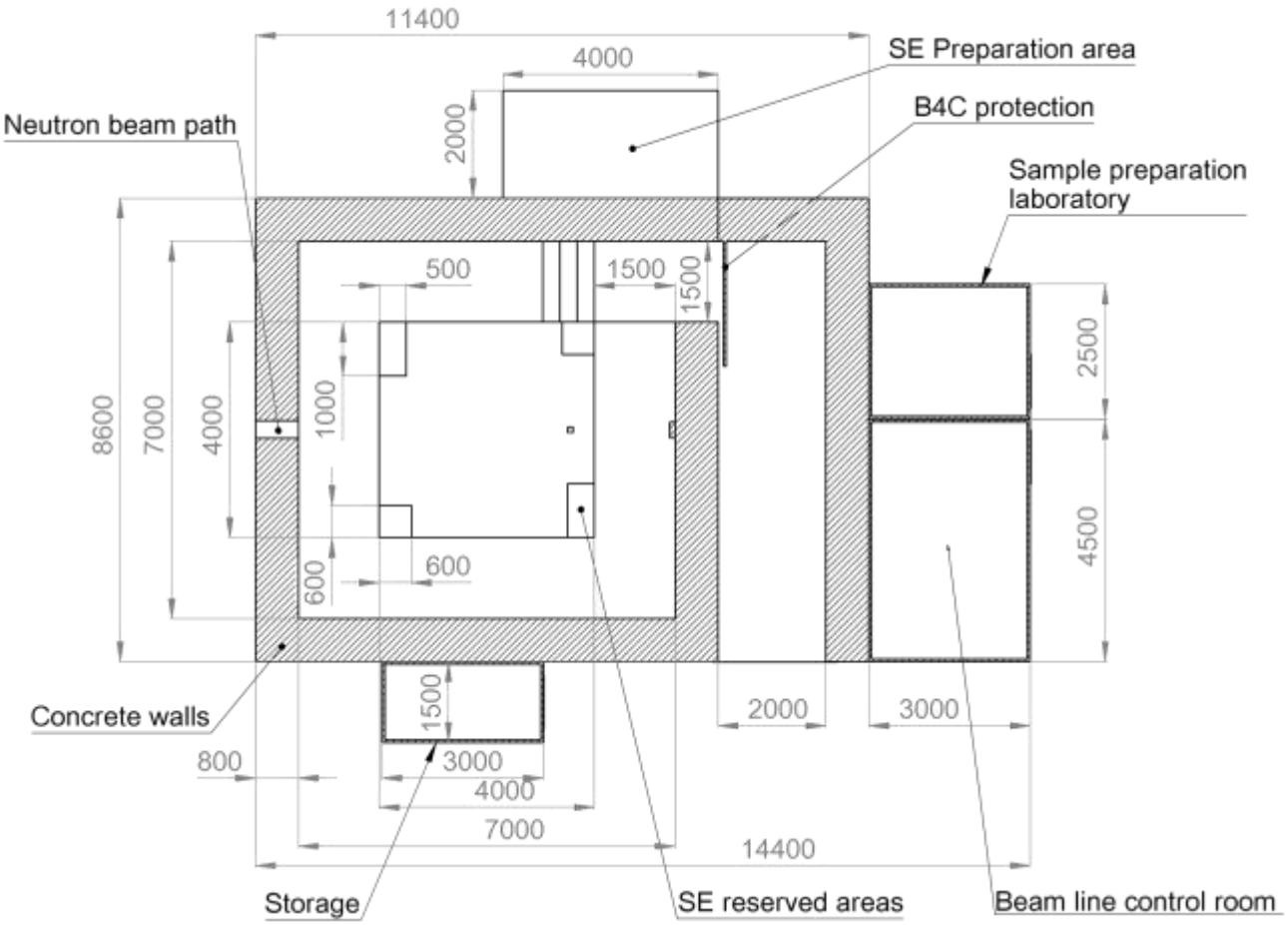

Figure 6.1.2: *Experimental cave 2D drawing*

6.2 Infrastructure (13.6.18.5.3)

A 16 m^2 area around sample position will be sur-elevated by 40 cm and made of polished concrete, allowing smooth detector positioning. The beam will be at 149 cm from the experimental cave floor allowing convenient access to the sample position to users and staff.

An aluminum platform, positioned above the detectors, will allow easy sample changing in tall sample environment such as a superconducting magnet.

A 1 T capacity crane with H-shape rails attached to the inside of the roof will enable handling of any component inside the cave and from the cave entrance door.

Utility distribution (power, cooling water, compressed air, gas distribution, vacuum, Ar/CO_2 detectors) will be available inside the cave, as close as possible to the sample area and at the vertical of either the gallery or one conduit.

6.3 Shielding (13.6.18.5.4)

The geometry of the cave is designed in such a way that the amount of shielding materials needed is reduced significantly. The closest distance between the sample and the wall will be 3.5 m. The vertical and horizontal concrete blocks will be 60 cm thick which is compliant with the maximum 20 T/m^2 floor load capacity. Borated layer (like Boral) or similar materials will be used to absorb thermal neutrons on the inner walls. Physical access to the experimental cave will require the opening of a light neutron absorber door equipped with 5 mm borated layer or equivalent. This door will be located at the entrance of the sample cave.

The '10x rule" (p.34 of NOSG Handbook, ESS-0039408) will be applied for the block assemblies. Special consideration will be provided for the shielding around the wall openings, such like beam entry, utilities, ventilation and etc. The beam stop will be located behind the detector assembly. It will absorb all the neutrons not scattered by the sample environments.

6.4 Sample cave access strategy

A corridor has been designed to avoid direct line of sight between the sample cave door and labyrinth entry. The labyrinth entry will be restricted by a fence interlocked with a NSS key. It will allow a minimum free surface of 1.5 m wide and 3 m high for components access. Outer walls of the labyrinth will be built from standard concrete blocks of 80 cm width.

6.5 Personnel safety system (13.6.18.5.1)

The experimental cave will comply with the PSS requirements to ensure maximum safety. A number of detectors (fire, O2 monitoring, water leak) will be installed along with a remote video surveillance system. The cave access routines and keys management practices will be developed following the ESS safety rules.

7 Shielding (13.6.18.1.9)

The beamline shielding for high-energy neutrons and prompt γ pulse has been calculated using the target, moderator and bunker model provided by ESS using MCNP. As these calculations are CPU time consuming and out of reach technically of most beamline teams, some beamlines are already using the MAGiC shielding as an input.

We would like to stress out that deep checking by the NOSG is mandatory to ensure that the used models are up to date with the last bunker and moderator designs. Failure to do so could potentially lead the ESS beamline shielding strategy to a disaster.

7.1 In-bunker shielding (13.6.18.1.9.1)

7.1.1 Shielding of thermal neutrons

5 mm thick boron carbide composite layer (Boral) will be used around the whole guide system inside the bunker. The goal here is to reduce as much as possible the thermal and cold neutron background to minimize activation of the bunker assembly as well as to protect the guide field magnets from incoming radiation.

7.1.2 Shielding of high energy neutrons and prompt γ pulse

The bunker is designed to shield the high-energy neutrons and the prompt γ-pulse coming from the target and moderators. The beamline does not need additional shielding from a safety point of view.

However, $Nd_2Fe_{14}B$ magnets have to be protected from high energy neutrons to avoid their demagnetization. An integrated flux of $1.3x10^{16}$ neutrons/cm^2 induces a 98% magnetization loss on $Nd_2Fe_{14}B$ magnets while a $2x10^{14}$ n/cm^2 flux induces a 10% loss [*A. Samin, Nuclear Instr. and Methods in Physics Research B, 342 (2015)*]. On MAGiC, the most sensitive device in this regards is the solid-state bender. The estimated neutron flux 4 cm above or below the direct beam at the light shutter position is of $4x10^6$ n/cm^2/s. At this rate, the saturating $Nd_2Fe_{14}B$ magnets will lose 10% of their magnetization in 2 years of operation at maximum power.

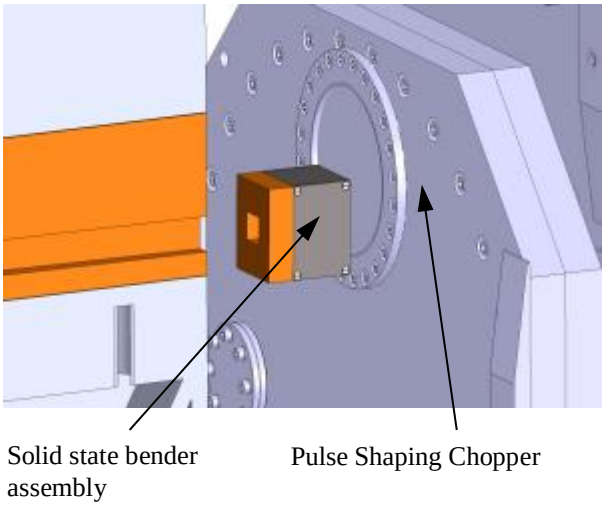

Fig. 7.1.2.2. *Shielding diaphragm of solid state bender. SSB is placed in between light shutter and pulse shaping chopper.*

To prevent such damages and limit maintenance, a copper or tungsten diaphragm will be placed in front of the whole bender assembly to scatter high energy neutrons over 4π sr. The size of the diaphragm window corresponds to the cross section of the bender (30x30mm). The diaphragm thickness will be in agreement with the available space between light shutter and chopper assembly (Fig.7.1.2.2).

As for the SSB magnets, the guide field magnets will have to be protected from the high-energy neutrons and prompt γ pulse. 20 cm of free space will be available between the magnet columns for this purpose. The current plan is to use copper or tungsten plates of 2 cm thickness up to the bunker wall.

7.2 High Energy Shutter (13.6.18.1.7.2)

MAGiC is a straight beamline up to the thermal polarizer. Maintenance during operation (beam on target) requires a high-energy shutter to cut the direct beam and maintain dose rate outside of the bunker below the 25 μSv/h limit.

The current design is based on a working solution developed by PSI and made of 6 vertical drums located inside the bunker wall. Each drum is 30 cm in diameter with an empty channel of 10 cm to insert the elliptic guide. The effective thickness of each drum is of 20 cm. Presently the high energy shutter is incorporated into the 3m thick bunker shielding.

MCNP calculations showed that a dose rate of 15 Sv/hr (see fig. 7.2) is expected at the bunker wall (24.5 m) that need to be reduced down to 25 μSv/hr to allow maintenance operation on downstream elements. With a drum sequence of: borax / steel / steel / borax / steel / tungsten, the expected dose rate outside of the bunker wall is reduced to 15.2 μSv/hr.

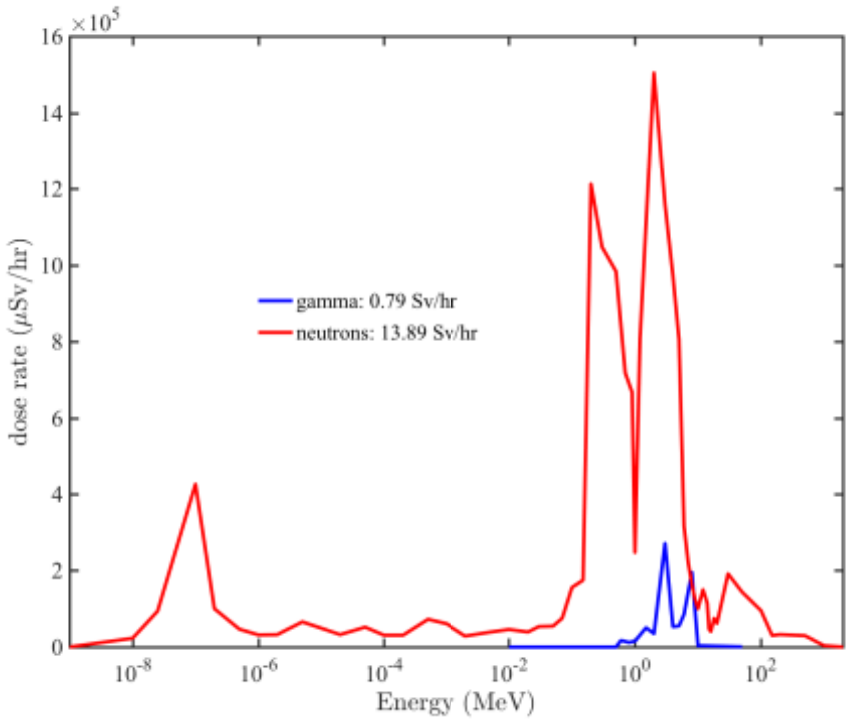

Figure 7.2: *calculated dose rate for neutrons and γs at the bunker inner wall position.*

This design is a preliminary design showing the feasibility of such a shutter. If no standard solution is proposed by the ESS during next year this design will be used on MAGiC.

7.3 Neutron guide shielding (13.6.18.1.9.3)

Two source of radiation have to be considered when calculating the neutron guide shielding. The first one is due to the spectrum transported by the guide system. The thermal and cold neutrons losses inside the guide have been simulated using McStas. The 5-mm thick boron layer will capture lost neutrons and emit 478 keV γ-rays. These γ-rays will be absorbed by the concrete shielding. The corresponding concrete mass attenuation factor μ/ρ is of 0.08915 cm^2/g [*http://physics.nist.gov/*]. A dose rate of 1.5 μSv/hr corresponds to a γ flux of 167 photons/s/cm^2 [*Tech. Report Jet Propulsion Laboratory, 32-439 (1963)*]. Figure 7.3 presents the minimal concrete thickness necessary to shield the generated γ-rays.

The second source of radiation comes from the high-energy neutrons emitted by the target and the prompt γ pulse. Neutron guide shielding calculations have been carried out using MCNP and a virtual source located at the bunker inner wall. This virtual source has been setup based on the transported spectrum from the target/moderator and is representative of the actual high energy and prompt γ spectrum. Using a virtual source dramatically speed up calculations.

Along the beamline, a 50x50 cm^2 air-filled channel has been simulated. The guide itself has been setup inside as a 10x10 cm2 section under complete vacuum.

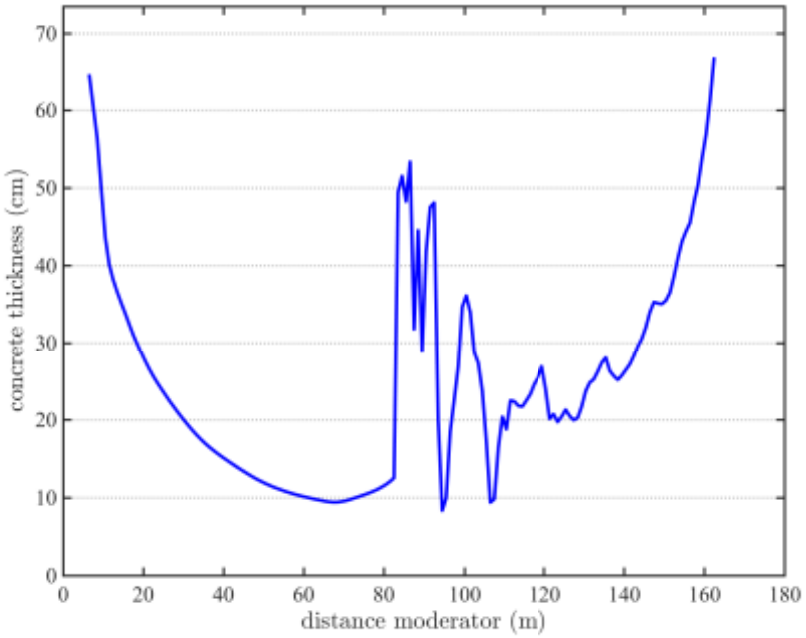

Figure 7.3: *concrete thickness necessary to shield the γ-rays induced by lost neutrons along the guide system.*

7.3.1 High energy: first half-ellipse

The first half-ellipse outside of the bunker wall offers a direct view of the moderator (28 m to 80 m). Several tallies were placed outside of the simulated shielding to follow the dose rates up to the thermal polarizer position.
The simulated shielding is composed of 10 cm of standard borated concrete (5% B_4C), 10 cm of standard steel and 50 cm of standard concrete (see fig. 7.3.1).

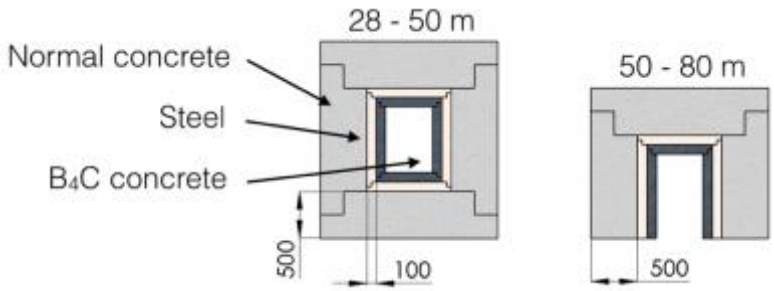

Figure 7.3.1: *simulated shielding along the first half-ellipse of the guide. In the bunker hall, a sur-elevated concrete structure will compensate the 2 m beam height to reduce shielding cost.*

The following dose rates were calculated outside of the shielding:

30 m: 3.4 µSv/hr
50 m: 1.9 µSv/hr
77 m: 1.1 µSv/hr

Some of these values are close to the 3 μSv/hr limit set by ESS. However, the bunker wall model used for calculations was missing a polyethylene layer and most of the dose rate at 30 m has been identified as leak from the bunker wall.

7.3.2 High energy: thermal Polarizer

The thermal polarizer is a hotspot regarding shielding as half of the thermal neutron beam will be lost at this position. This is also the last part of the instrument were a direct view from the moderator will be possible. Finally, the band chopper is currently located at this position. The simulated shielding at this position was of 50 cm of heavy borated concrete (5% B_4C, density=4.9 g/cm^3). Outside of the shielding a dose rate of 1.6 μSv/hr has been calculated. To ensure safety, the current plan is to use 80 cm of borated heavy concrete along the 4 m of the thermal polarizer and around the Band Chopper.

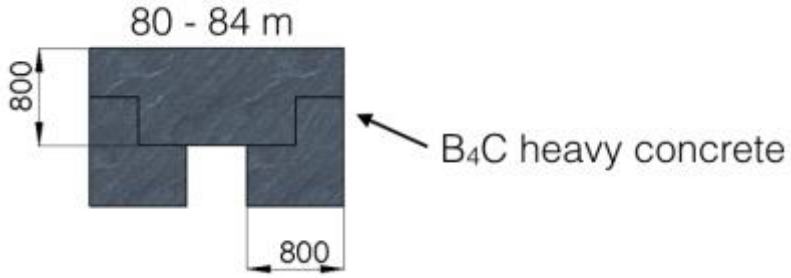

Figure 7.3.2 *simulated shielding around the thermal polarizer.*

7.3.3 High energy: second half-ellipse

At this stage of the instrument, no direct line of sight from the moderator remains. The shielding up to the experimental cave is therefore identical to the one used at reactor source (ILL).
The simulated shielding was of 50 cm of normal concrete. 2 m after the thermal polarizer, a dose rate of 1.3 μSv/hr has been calculated. At 150-m a dose rate of 0.2 μSv/hr has been calculated inside the shielding.

However, neutron losses inside the guide will need up to 70 cm of standard concrete to properly shield the emitted γ-rays.

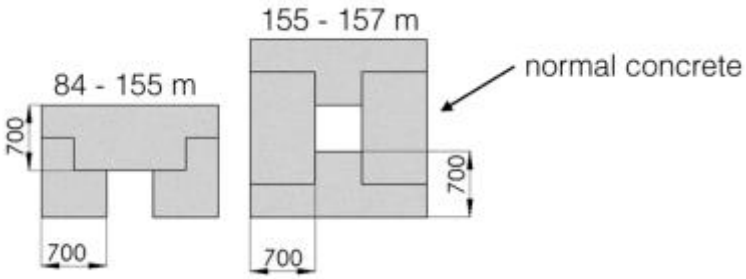

Figure 7.3.3 *simulated shielding around the second half-ellipse, up to the experimental cave.*

7.4 Experimental cave shielding

7.3.1 Fast shutter

The experimental cave will be equipped with a dedicated fast shutter capable of blocking the incident beam. This shutter will be connected to the PSS. Exact specifications will be defined during the details design phase.

7.3.2 Beam stop

The current beam stop design consist of a 10x10x10 cm^3 boron carbide volume surrounded by 5-cm of lead and enclosed in a 10-cm heavy concrete housing. The total volume occupied is of 40x40x40 cm^3. The beam stop will be directly connected to the evacuated flight path. A lead sheet will be placed in front of the beam stop to prevent γ-ray propagation back to the detectors. This lead part is fairly transparent to neutrons and will not endanger safety.

The neutron beam will be captured by the boron carbide volume. As a result, 478 keV γ-rays will be emitted. Considering a beam of 10^{10} n/s, this corresponds to $1.67x10^7$ photons/s/cm^2 outside of the boron carbide. After 5 cm of lead, this number is down 442 photons/s/cm^2. After an additional 10 cm of concrete, hence outside of the beam stop, only 13 photons/s/cm2 are transmitted corresponding to 0.08 µSv/hr. The hottest point would be the backward direction as only the 5-cm lead part will be in the γ path.

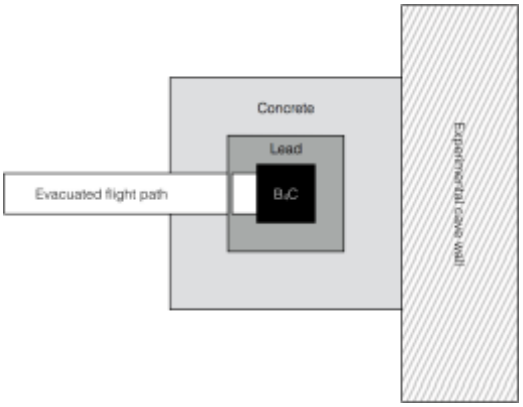

Figure 7.3.2: *sketch of the MAGiC beam stop.*

7.3.3 γ and scattered neutrons shielding

The first source of radiation inside the experimental cave will be γ-rays resulting from the capture of thermal neutrons by various elements. The optimal thickness of the experimental cave walls has been calculated based on a $1x10^{10}$ n/s neutron flux at sample position (100% increase compared to the calculated beam). The worst-case scenario of the total beam being converted to 2 MeV γ-rays has been used.
The dimensions of the experimental cave will spread the γ-rays over 264 m^2 down to 3.75 $x10^3$ γ/s/cm^2 on the inner walls. To comply with the 1.5 µSv/hr limit, the γ flux has to be reduced down to 54 γ/s/cm^2 (~ 100 reduction factor).

The mass attenuation coefficient of concrete for 2 MeV γ-rays is of 0.04557 cm^2/g [*http://physics.nist.gov/*]. To achieve 1% of effective transmission a thickness of 42 cm is necessary. A safety factor of 10 has been applied to the calculated value yielding a 60-cm wall thickness.

The second source of radiation is the scattered beam. A calculated flux of $4x10^9$ $n/s/cm^2$ is foreseen at sample position. The worst-case scenario considered is the case of a graphite monochromator placed at sample position. Based on the incident divergence and the typical mosaicity of a sample, 4% of the total flux could be scattered in one specific direction and spread over 10 cm^2 on the cave inner wall. This roughly corresponds to $2x10^7$ $n/s/cm^2$. The thermal spectrum is centered around 1.2 Å. Considering the transmission of a boron carbide layer, a thickness of 5 mm will be sufficient to reduce the transmission down to 10^{-6}. The current plan is to cover the entire experimental cave walls and roof with 5 mm of boron carbide layer. Additional calculations are necessary to optimize the boron carbide layer positioning in order to reduce costs.

8 Preliminary Safety Analysis for the instrument

The main hazard present at the instrument is ionizing radiation. The shielding (see section 3.5) protects personnel outside the instrument from radiation hazards. For changing samples users need to have access to the experimental cave without being exposed to radiation. For maintenance purposes, all parts of the instrument also shall be accessible to ESS staff. This is achieved safely with the beam cut off system, which consists of heavy shutter and beam stop. The light shutter located immediately outside the target monolith stops radiation emanating from the target, when the proton beam is not on target and allows maintenance work to be performed on downstream components. The light shutter is not a part of the MAGiC work package; however, our team will contribute to the optics elements installed inside this shutter.

The heavy shutter is located at about 24.5 m from the moderator, inside the bunker. It blocks the neutron beam and therefore allows the personnel access to the downstream elements (guide, polarizer, chopper, experimental cave). The heavy shutter is connected to a Personnel Safety System (PSS) that interlocks the areas (such as the experimental cave) when the shutter is open. Additional radiation alarm will be installed inside the cave. It will be connected to PSS to prevent personnel entering the experimental cave if a radiation leak has been detected.

A search procedure ensuring that no people are inside is required to close the interlock and open the shutter. All interlocked spaces shall have emergency stop buttons that close the appropriate shutters to prevent radiation exposure. All shutter systems are designed to fail closed.

Other safety systems which are not related to radiation hazard include: (i) fire detection and automatic fire extinguishing that will be installed inside the control hutch, sample preparation area and experimental cave; (ii) oxygen deficiency sensor will be installed within the experimental cave. Additional sensor will be installed in vicinity of the sample position to monitor oxygen levels during liquid helium and nitrogen refills of SEE. In case when inert gases are used for the user experiment portable sensors will be placed around the experimental setup.

The warning signs indicating radiation, cryogenics and high magnetic fields hazards will be positioned around the instrument and a first-aid kit will be available for users in the instrument hutch.

The administrative control will include training of all users and personnel working at the instrument. The training will include the walkthrough of the instrument, identification of all potential hazard situations and appropriate response. All training materials will be available on the instrument website. The hard copies of those documents will be available at the control hutch.

9 Software components

9.1 Instrument control

The software controlling the beamline will be developed by the DMSC as their contribution to the instrument project. Several modes have to be proposed to the users and beamline staff.

For the general users, an intuitive GUI is mandatory. Only the most relevant options should be proposed, allowing to simply change temperature, magnetic field and setup a data collection (steps, time, resolution).
For advanced users, a scripting solution should be proposed. The trend today is to offer Python scripting. This scripting solution should evolve versus time to adapt to the possible new trends.
For beamline staff, a complete scripting and CLI solution shall be developed. This mode is the easiest one to remotely control the instrument.
For the beamline staff, a full GUI access to the instrument shall be proposed remotely.

9.2 Data visualization

Data visualization should be done in real-time. At least two view shall be offered to the users:

1) A Laue pattern view updating in real-time and allowing to quickly check a sample quality and the progress of the experiment.
2) A 3D Q-space view allowing to slice the collected dataset along specific directions. To do so, parts of the data reduction have to be implemented, such as the orientation matrix refinement.

The first visualization is trivial and will not require a huge processing power. The second one is mode CPU intensive as the collected datasets will be memory consuming. Nevertheless, these two tools are mandatory for operations.

9.3 Data reduction

Data reduction is the process of extracting a list of HKL from the raw collected datasets. The following steps are necessary for each collected event:

- Normalize for detector efficiency and spectrum distribution: the detector efficiency has to be done at every cycle start. It is usually done using a Vanadium sample. The spectrum distribution is collected on the incident beam monitor.
- Correct for the Lorentz factor: to compare events collected at different wavelength and angle positions, the $\lambda^4/sin^2(\theta)$ correction has to be applied.
- Correct for sample absorption: in the case of non-spherical samples, the sample geometry has to be described in order to correct the collected intensities for absorption. The easiest way would be to make a 3D model of the sample and use the orientation matrix to automatically calculate this parameter.

- Correct for extinction: in the case of perfect crystals, the relative intensities between reflections can be strongly affected by extinction. With a multiple wavelength instrument, it should be possible to automatically and efficiently correct for extinction.
- Convert each event to Q-space and reorder Q-space by density: this is the first step to find Bragg reflections.
- Find the orientation matrix: a fast Fourier transform on the highest density points allows to refine the lattice parameters, lattice angles and sample orientation relatively to the instrument axes. This step will also detect possible propagation vectors for the magnetic structure.
- Predict the position of all relevant peaks.
- Integrate scattered intensities: Mulitple algorithm are available.
- Export to "hkl int error λ orientation" ascii file for analysis.

Since every spallation source is operating a single crystal diffractometer, a lot of efforts have been put into the data reduction algorithm. In particular, Mantid is now well suited for the job and every step should be functional by the time MAGiC will be operational. However, this process has to be as intuitive as possible. Most of the options should be hidden to the average user and the reduction process should be as automatic as possible. This is the key for instrument productivity and user enthusiasm.

One has to keep in mind that the datasets collected at ESS will be one order of magnitude larger than actual datasets collected at spallation source. At least a few hundred gigabytes and up to a few terabytes of data will be generated for data reduction. Efforts have to be made to reduce the time required by this process through routines optimization, correct scaling of memory and increase in cpu power. As of today, some operations are longer than the actual experiment which is killing instrument output.

Users will start data reduction during the experiment. However, a remote solution shall be proposed to allow further data reduction from the user home institution. In the ideal case, users will go back to their home institution with the complete set of reduced data.

9.4 Data analysis

Data analysis is the last step before publication. The reduced data are compared to numerical models, and a minimization algorithm trying to find the best physical model reproducing the data. As of today, multiple software suites can be used at this effect.

For magnetism, JANA2006, FULLPROF or the CCSL are workable solutions. JANA2006 is already capable of treating single crystal spallation source reduced data and has been updated to natively work with TOPAZ datasets. FULLPROF and the CCSL will need fully reduced datasets to be productive.

An effort is currently made to find a common language for magnetic structure definition. A magnetic CIF format is under development and is strongly supported by the different actors.

In particular, the team behind the Bilbao crystallographic server, is actively working on the subject.

10 Expected performance at 2 MW

The MAGiC performance have been estimated during the phase 0 based on the pancake moderator design at 5 MW power, and the full scope instrument configuration. The results presented in this section are based on these simulations and have been scaled as follow:

- The number of steps necessary for a full data collection is 3 times higher on half-polarized experiments to account for the large detector coverage reduction decided during the scope setting meeting (60° instead of 160°).
- The acquisition time is 2.5 times more important to compensate for the source power reduction.

Compared to the proposal, the acquisition time are therefore 7.5 times longer.

Each simulated experiment consists of a full sample rotation around the Z axis. 180 steps have been performed, each of them corresponding to a one second acquisition in McStas. A specific cylindrical TOF component has been used. This component works in "*events mode*", stores data in binary mode, and is as close as possible of a real data acquisition. A typical dataset is several Go large.

The collected data are extracted and corrected for Lorentz factor in MATLAB. Corrections for detectors efficiency, sample volume, silicon SSB transmission and polarization analyzer transmission (estimated to 30%) are applied at the same time. The data are finally integrated and converted to a (H, K, L, I, dI) list that can be used for data analysis.

10.1 Diffuse magnetic scattering including polarization analysis

The configuration validated for construction during the MAGiC scope setting meeting includes the full polarization setup. The anticipated performance is the one expected for the full scope configuration and the foreseen upgrades will not increase the instrument performance in this regard.
To benchmark the capacity of MAGiC in diffuse scattering we have chosen the spin ice $Ho_2Ti_2O_7$, which was measured on D7 (ILL) using a monochromatic beam and polarization analysis [*Science 326, 415-417 (2009)*]. The relative instrument efficiencies can be essentially estimated by the flux ratios of their cold spectrum ($7.0x10^8$ vs $2x10^6$), although one could foresee possible flux gains of the D7 upgrade in the ILL endurance program.
The diffuse scattering cross-section was simulated using the analytical model from Henley [*Ann. Rev. Condens Matter Phys. 1:179–210 (2010)*]. The simulations use the full pulse of polarized neutrons from the cold moderator ($2.0<\lambda<3.7$Å). We chose a small crystal of only 10 mm^3, which could provide also useful integrated Bragg intensities in the same measurement. 180 Laue patterns have been simulated, with 2° steps of sample rotations and 15 secs acquisition time per step (after corrections). Within the total counting time of 45 min. for a full rotation, one obtains ~10^3 counts near a diffuse peak in a dQ^3 element of 3×10^{-4} $Å^{-3}$,

which is the estimated volume for a D7 detector cell. The estimated gain factor is of two order of magnitude. The simulated diffuse scattering is shown in Fig. 10.1.

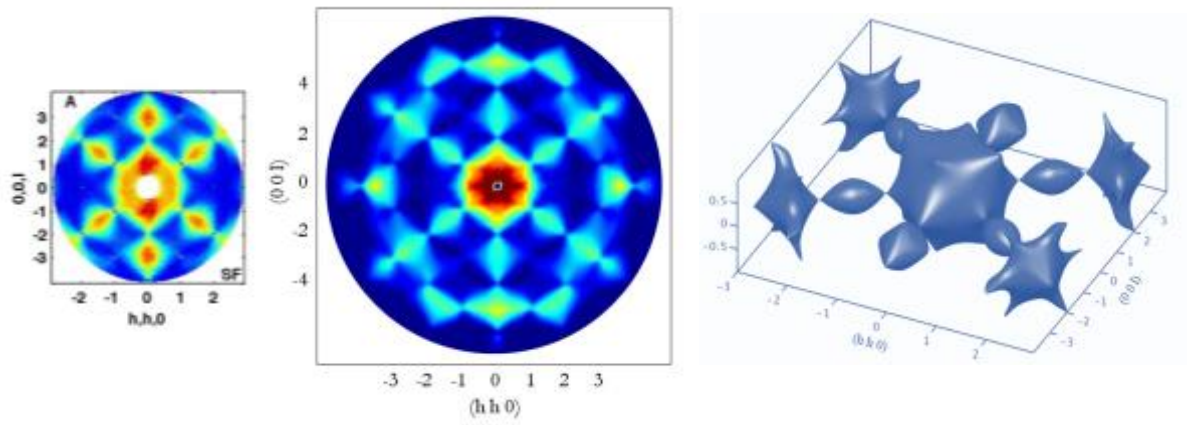

Figure 10.1: *Spin ice diffuse scattering of $Ho_2Ti_2O_7$. (left) data from D7 (λ=4.8Å) (center) Simulation on a 10mm^3 crystal on MAGiC (2.1-3.8 Å). (right) a section of the 3D iso-surface reconstruction from the MAGiC data without polarization analysis.*

More features are revealed with extended Q-range (vertical Q_z<1.6Å^{-1}) and 3D-resolution (dQ_z~0.02 Å^{-1}), in particular, when using the large detector bank without polarization analysis. For illustration purpose, one of the equal intensity surfaces (iso-surface) obtained in the simulation is shown in Fig. 10.1. Note, such an option for a large position sensitive detector exists nowadays at the similar instrument DNS at MLZ. It yields valuable 3D information about frustrated systems with local constraints.

10.2 Structure determination using polarized neutrons

One of the core capabilities of MAGiC will be magnetic structure determination under magnetic field.

We used the **molecular magnet** $Cu_2(NC_9H_{13})_4(N_3)_2(ClO4)_2$ as a benchmark reference for a magnetic structure determination in the half-polarized setting, which measures the interference of nuclear and magnetic structure factors. The simulation gives a very challenging example from a today's perspective, because it contains only two unpaired electrons per formula unit consisting of 110 atoms including 52 hydrogen ones. A relatively large number of reflections is required due to the low symmetry of the monoclinic structure $P2_1/c$ with a=12.39, b= 13.03, c=12.69 Å and γ=98.4°.

We used the model predicted by DFT as an input of the scattering law for the McStas sample module, a sample size of 10 mm^3, and simulated an experiment with a full sample rotation and a total of 2 hours beam time. We obtained 600 useful reflection, with R-1>**3σ,** for thermal setting of the instrument, reproducing successfully all features reported in literature. The reference work took two weeks of beam time on D3 which is a single counter diffractometer. Nowadays it could already be done within 2 days on VIP at LLB using a large

2D detector. The estimated gain factor is of 2 order of magnitude compared to VIP at LLB and 3 order of magnitude compared to a single counter diffractometer.

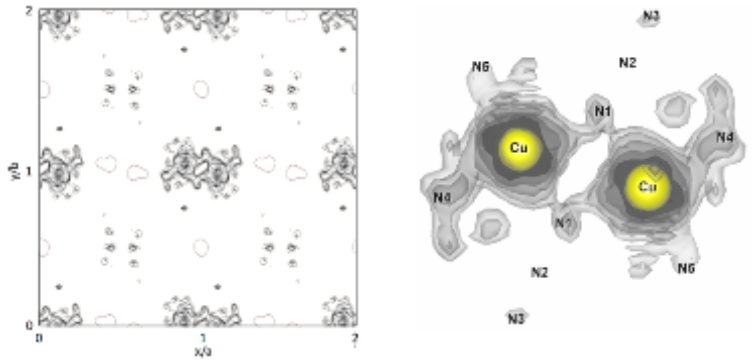

Figure 10.2: *The spin density map of a molecular compound reconstructed by Maximum Entropy Method from MAGiC data.*